JOURNAL OF MATERIALS SCIENCE **38** (2003) 4783–4801

High-temperature thermal barrier coating formation by laser alloying of CP-Ti with pre-placed Ni-SiC coating

J. S. SELVAN, K. SUBRAMANIAN
Department of Physics, Anna University, Chennai 600 025, India
E-mail: crystal@sirnetm.ernet.in

High-temperature thermal barrier coating was created on CP-Ti using a pre-placed Ni-SiC layer by laser alloying technique. The coating was developed using 80% Ni + 20% SiC, 50% Ni + 50% SiC and 60% Ni + 40% SiC, and the latter two compositions are found to be efficient in producing a uniform layer. The 100% SiC pre-placement was also used. A flaw-less coating of 0.4–0.6 mm thickness was produced at a lower power density of 1.3 to 1.9×10^5 W cm^{-2}. Very high power density of 2.5–3.0 $\times 10^5$ W cm^{-2} is inefficient to produce uniform coating. The laser alloyed coating consists of dendrites and intermetallic precipitates. The degree of dendrite population depends upon the coating composition and laser processing conditions. The coating hardness was 600–1200 HV, which is three to six times higher than the base titanium. Uniform hardness was obtained for the coatings produced at a laser power density of 1.3×10^5 W cm^{-2}. The titanium silicide (TiNiSi, Ti_5Si_3, TiSi) and nickelide ($NiTi_2$) phases formed on the laser-alloyed coating surface was confirmed by X-ray analysis. These intermetallic phases can improve high-temperature properties of titanium and its alloys. The effect of laser power density and coating composition on the alloying depth alloying width, hardness and microstructure are discussed. The present work investigated the microstructure evolution, hardness and compound phases by means of optical and scanning electron microscopy, Vickers hardness testing, EDXRD and SIMS analysis. A 5 kW CW CO_2 laser was used for laser alloying experiments.

1. Introduction

Gas turbine components (GTCs) used in aircraft, marine and power generation equipments are subjected to high stress under complex thermal, mechanical, corrosive and erosive environments [1]. The prolonged exposure of aero engine GTCs at a high-temperature 2500 F leads to surface degradation due to the reaction of gas stream particles in combustion gases with engine surface [2–4]. In aircraft industries the high-temperature coatings are demanding because failure of GTC can bring dramatic structural collapse to the aircraft and therefore safety of the aircraft is questioned. These problems can be minimised by applying protective coating (thermal barrier or high-temperature coating) to the gas turbine components. Coating techniques such as electroless plating, pack cementation, PVD, CVD, thermal spray, low pressure plasma spray and self propagating high-temperature synthesis have been employed to provide thermal barrier coatings for improving high-temperature corrosion and erosion resistance of aero engine GTCs [2, 5–9]. Laser alloying and cladding is a fairly new improved method to deposit a high quality thermal barrier coatings [10].

Thermal barrier coating for GTCs should have the following characteristics [11–13]:

- resistance to hot corrosion
- resistance to thermal cyclic oxidation
- resistance to thermal fatigue cracking
- resistance to erosion/impact strength
- excellent thermal stability
- long term diffusional stability
- strong adhesion to the substrate;
- sufficient thickness
- good uniformity and coherence
- ease of application
- compatibility with the substrate and
- good self healing capability.

Many thermal barrier coatings based mainly on aluminides, MCrAlY (M = Co, Ni, Fe) and ceramics [14, 2] were developed to extend the performance of high-temperature GTCs. In the initial stage, simple diffusion aluminide and metal modified aluminide coatings such as platinum aluminide, nickel aluminide, platinum modified rhodium aluminide, manganese plus chromium modified aluminide coatings were used [15]. Recently the MCrAlY alloy (M = Ni, Co, NiCo) has been evolved as a thermal barrier coating material for the protection against high-temperature corrosion and oxidation [16, 3]. Nickel based metal and ceramic

coatings such as NiCr, NiCrSi, NiCrSiB, NiCrHf, NiCrHfAl, NiCoCrAlY, NiCoCrAlHfSiY, $NiCrCr_2O_3$ and $NiCoCrAlY/TiB_2$ have also been employed as corrosion and oxidation resistant coatings to high-temperature components [2, 3, 16, 17]. Nowadays attention has been paid towards the high-temperature ceramics ZrO_2-Al_2O_3 and ZrO_2-Y_2O_3 for hot corrosion resistance of GTCs [10].

SiC ceramic has excellent resistance against creep, fatigue, thermal shock, oxidation, corrosion, impact and erosion behaviours and it has high stress to rupture values [18]. The refractory ceramic SiC when alloyed with nickel or titanium can produce a composite material [19–22]. This composite can be used as a coating material to attain the service temperature of 2000 °C [23]. The Ni-SiC coating can give chemical stability and prevents high-temperature corrosion and erosion damage of GTCs and it can be considered as an alternative choice of thermal barrier coating for GTCs.

Ni-SiC and Ni-P-SiC composite coatings have been developed by the electro-deposition process and the coating was found to have excellent corrosion and wear resistances [24, 25]. The powder dispersed Ni-SiC metal ceramic coating is used in parts subject to friction and can be applied to all kinds of reciprocating engines operating under severe conditions which have good abrasion resistance and slip properties [26]. The coatings applied by electro-deposition, CVD and PVD processes generally results in poor adhesion to the substrate, small layer thickness and lengthy processing duration. Whereas, the laser process has the ability of giving flawless coating with excellent adhesion to the substrate which is one of the essential reqirements for thermal barrier coating development. The high quality thermal barrier coating was developed successfully on nickel base super alloy turbine blades using laser cladding process by Rolls Royce Company, USA [10]. To improve the high-temperature behaviour of SS-4Cr-13 alloy, Pei *et al*. [27] have developed Ni based alloy composite (Zr_2O_3-Y_2O_3/Ni) coatings on 4Cr-13 substrate by a laser cladding process.

On the basis of these observations, in this work an attempt has been made to produce a thermal barrier coating for improving the high-temperature behaviour of titanium by means of laser alloying with Ni-SiC composite powder. Using this process the high-temperature property of titanium can be improved by producing Ti/Ni-SiC metal matrix composite and high-temperature intermetallic silicide formation. The primary aim of this study is to determine whether the laser alloying process could produce flawless, dense, uniform, thick coatings on CP-Ti substrate. To accomplish this objective, various combinations of laser parameters and coating compositions were attempted. For comparison, pure SiC coating on CP-Ti was also laser alloyed at various processing conditions.

In this chapter, the effect of various coating combinations such as 50% Ni + 50% SiC, 60% Ni + 40% SiC, 80% Ni + 20% SiC and 100% SiC are discussed with respect to the surface features, alloying depth, compound phase formation, microstructure evolution and hardness behaviour. The laser power density is optimised for producing a good composite layer based on Ni-SiC coating.

2. Processing detail and characterisation

Laser alloying was carried out using 80% Ni + 20% SiC, 60% Ni + 40% SiC and 50% SiC + 50% Ni coating on commercial purity titanium (CP-Ti). For comparison studies 100% SiC was also laser alloyed on CP-Ti. The SiC and Ni powder were taken in appropriate weight proportions, blended in 10% PVA solution and pasted on titanium substrate. A 5 kW CW CO_2 laser (indigenously made at Centre for Advanced Technology, Indore, India) was used for laser alloying experiments. The laser processing parameters used in this study were given in Table I. Argon gas was used as a cover gas, which blew through coaxial and off-axis nozzles. After laser alloying, the samples were sectioned, mounted in epoxy, polished and etched in Kroll's reagent.

The laser alloyed specimens were characterised using hardness testing, microstructural analysis by optical microscopy, scanning electron microscopy (SEM), phase identification through energy dispersive analysis using x-ray (EDXRD) and chemical analysis using secondary ion mass spectrometry (SIMS).

2.1. Hardness testing

The mechanical property of laser alloyed surface was evaluated using Vickers hardness testing (Shimadzu's microhardness tester, HMV-2000, Japan). The hardness were measured on polished transverse sections of the laser alloyed track starting from the surface region and proceeding towards the unmelted parent material with an interval of 50 μm or 100 μm between two

TABLE I Laser processing parameters and estimated surface temperature values for SiC and Ni

Laser power kW	Beam dia. mm	Travel speed m min^{-1}	Interaction time s	Power density 10^5 W cm^{-2}	Energy density kJ cm^{-2}	Surface temp. for CP-Ti T °C	Surface temp. for Ni T °C
1.0	1	0.5	0.12	1.3	15.6	2131	2379
1.0	1	1.0	0.06	1.3	7.8	1791	2130
1.0	1	1.5	0.04	1.3	5.2	1572	1969
1.5	1	0.5	0.12	2.0	24.0	3061	3433
1.5	1	1.0	0.06	2.0	12.0	2550	3058
2.0	1	1.0	0.06	2.5	15.0	3310	3987
2.0	1	1.5	0.04	2.5	10.0	2872	3665
2.5	1	1.0	0.06	3.0	18.0	4069	4915

indentations. The Microhardness test was carried out using 200 gf load for 15 seconds.

2.2. Microstructure analysis

The microstructure of the laser-alloyed surface, HAZ, and base metal were analysed using optical microscopy and scanning electron microscopy (SEM) techniques. The etched polished samples were used for metallography studies. Olympus camera (PM-10M Photomicrographic system, Olympus optical Co., Ltd, Japan) attached to a Shimadzu microhardness tester was used to photograph the microstructure images. In SEM, the secondary electron image was used for microscopic analysis.

2.3. Phase identification-EDXRD

To identify the compound phases formed on the laser-alloyed surface, X-ray diffraction study was carried out using EDXRD method. The analysis was performed using a polychromatic x-ray beam from a copper target of a rotating anode x-ray generator (Rigaku Rotoflux, RV 200 B, Japan). A Very intense x-ray beam produced by operating the instrument at 50 kV and 50 mA was focused with a collimator of internal diameter 0.3 mm. A well-collimated X-ray beam 300 μm in diameter was projected on the laser alloyed surface at constant angle of 15°. The diffracted ray from the alloyed surface was collected by Germanium detector (CANBERRA, S100, USA). Measured values were processed with the assistance of a Pentium II computer interfaced with the Multi Channel Analyser and the diffractometer. The collected data were indexed using XRDA (a program to analyse energy and angular dispersive x-ray diffraction patterns) software package. After the usual smoothing (quadratic smoothening) and peak search operations, the phases formed on the LAC surface were identified by comparing the indexed data with the JCPDS files [28].

2.4. Chemical analysis - SIMS method

The diffusion of coating or alloying elements in the laser-alloyed region was investigated using the secondary ion mass spectrometry (SIMS) technique. The machine used was CAMECA ims 4f (CAMECA instruments, Inc., Trumbull, USA). The finely polished and etched samples of 10×5 mm size was used. Before SIMS analysis the sample surface was cleaned with acetone. The analysis was made with a Cs^+ primary ion beam operated at 10 keV. By using a double focusing spectrometer (energy sector followed by a magnetic mass analyser), the emitted secondary ions were analysed and subsequently collected by the electron multiplier. Line profile analysis was made across the laser-alloyed cross section.

3. Results

3.1. Surface conditions

The details of surface quality (smooth or rough), cracking behaviour and porosity of all the coatings created by laser alloying of the CP-Ti with 100% SiC, 50% Ni + 50% SiC, 60% Ni + 40% SiC and 80% Ni + 20% SiC are given in Table II. At lower energy density 1.3×10^5 W cm^{-2}, a smooth surface was observed at 80% Ni + 20% SiC and 60% Ni + 40% SiC coating conditions. Surface alloying produced a rough surface and a deep undercut behaviour at all coating conditions when laser alloying was carried out at higher energy densities of 2.0 and 2.5×10^5 W cm^{-2}. When alloying was performed using 100% SiC, cracking was observed inside the laser alloyed coating (LAC). By the addition of nickel with SiC no cracks were initiated inside the LAC and the crack initiation was reduced to very high level. Porosity scarcely resulted in all the processing conditions.

3.2. Alloyed layer configuration

The melt pool configuration of the laser-alloyed surface was examined using optical microscopy at 50× magnification and it has a bowl like appearance at low power densities 1.3 and 1.9×10^5 W cm^{-2}. At high power densities 2.5 and 3.0×10^5 W cm^{-2} a wine cup and deep weld like morphology was observed.

Fig. 1a–c shows the melt pool configuration of the laser-alloyed surface using 100% SiC at laser power densities 1.3×10^5 W cm^{-2} (q-1.0 kW, d-1 mm, v-0.5 m min^{-1}), 1.9×10^5 W cm^{-2} (q-1.5 kW, d-1 mm, v-1.0 m min^{-1}) and 2.5×10^5 W cm^{-2} (q-2.0 kW, d-1 mm, v-0.5 m min^{-1}), respectively. From Fig. 1a–c, it can be seen that the alloying depth was found to increase with the increase of laser power density. Fig. 1a and c show a bowl and wine cup like surface profile, respectively. The melt pool configuration of the laser-alloyed CP-Ti with 80% Ni + 20% SiC coating at power densities 1.31, 1.91, 2.5 and 3.0×10^5 W cm^{-2} were shown in Fig. 2a–d, respectively. In this case, the bowl and a deep weld like profile was formed at low and high power densities, respectively. By comparing all the alloyed layer cross section shown in Fig. 2a–c, it is seen that as the power density increases the depth and width of the melt pool increases and this was due to the successive increase in heat input. The increase in surface temperature tends to produce a key-hole behaviour. Due to the multiple reflections within the key-hole the energy absorption increased, which tends to increase the alloying depth and width.

3.3. Alloying depth

In the laser alloying process, it is a fact that at a fixed beam power and diameter, increase in the scan speed decreases the alloying depth. Also, at a constant interaction time the alloying depth increases with the increase of incident laser power density. The effect of alloying depth on the chemical composition can not be generalised. In this study, the effect of nickel composition on alloying depth was investigated. From Fig. 3, it can be seen that the alloying depth was found to increase with the increase of nickel concentration. The alloying depth was found to be 0.35 mm for a 100% SiC coating condition. It slightly increased to 0.45 mm when nickel and SiC was taken in equal weight proportions. When a high nickel content of 80 wt% was added to

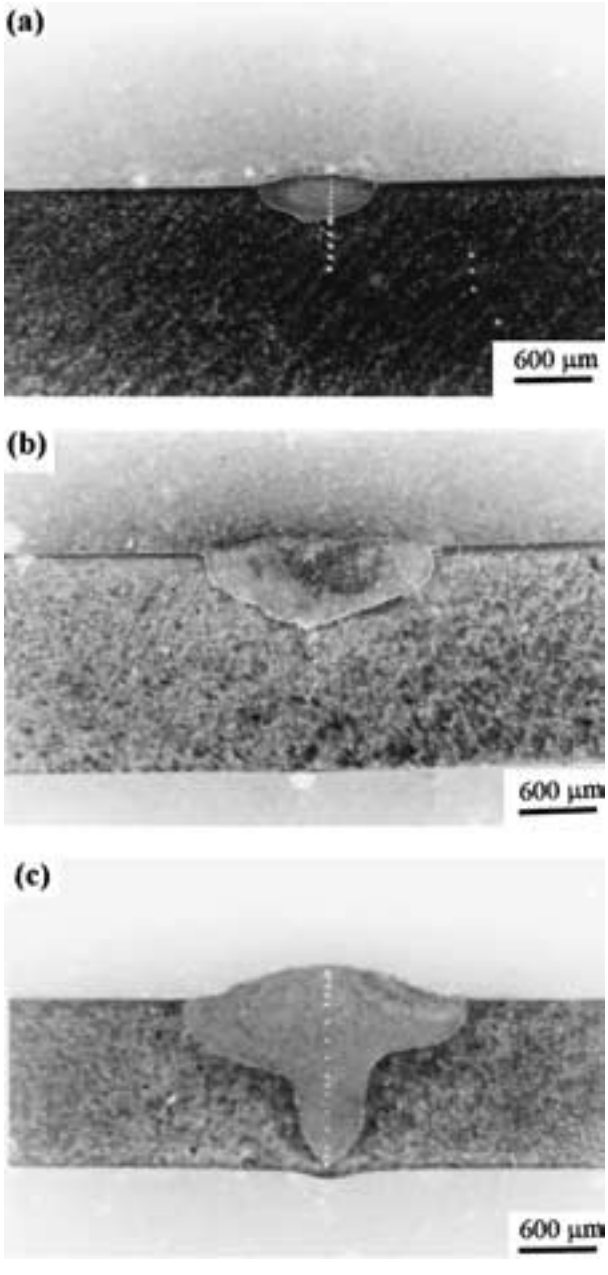

Figure 1 Transverse cross section of laser-alloyed CP-Ti with 100% SiC at power density (a) 1.3 (b) 1.9 and (c) 2.5×10^5 W cm^{-2}.

SiC, the alloying depth steeply increased to 1.1 mm. It is believed that the addition of nickel can activate the energy absorption and heat transfer efficiency, which might have resulted in larger alloying depth.

3.4. X-ray diffraction analysis

The phases formed on the laser-alloyed surface were investigated using x-ray diffraction study. Fig. 4a shows the EDXRD spectrum of unmelted CP-Ti, in which the peaks corresponding to α-Ti were identified. No oxide peaks were revealed in the x-ray diffraction results. The EDXRD spectrum of CP-Ti alloyed with pre-placed 100% SiC, 50% Ni + 50% SiC, 60% Ni + 40% SiC and 80% Ni + 20% SiC coatings are shown in Fig. 4b–e, respectively. An analysis of the peaks observed in the CP-Ti alloyed with 100% SiC (Fig. 4b) shows that the alloyed layer consists of three phases namely (a) solid

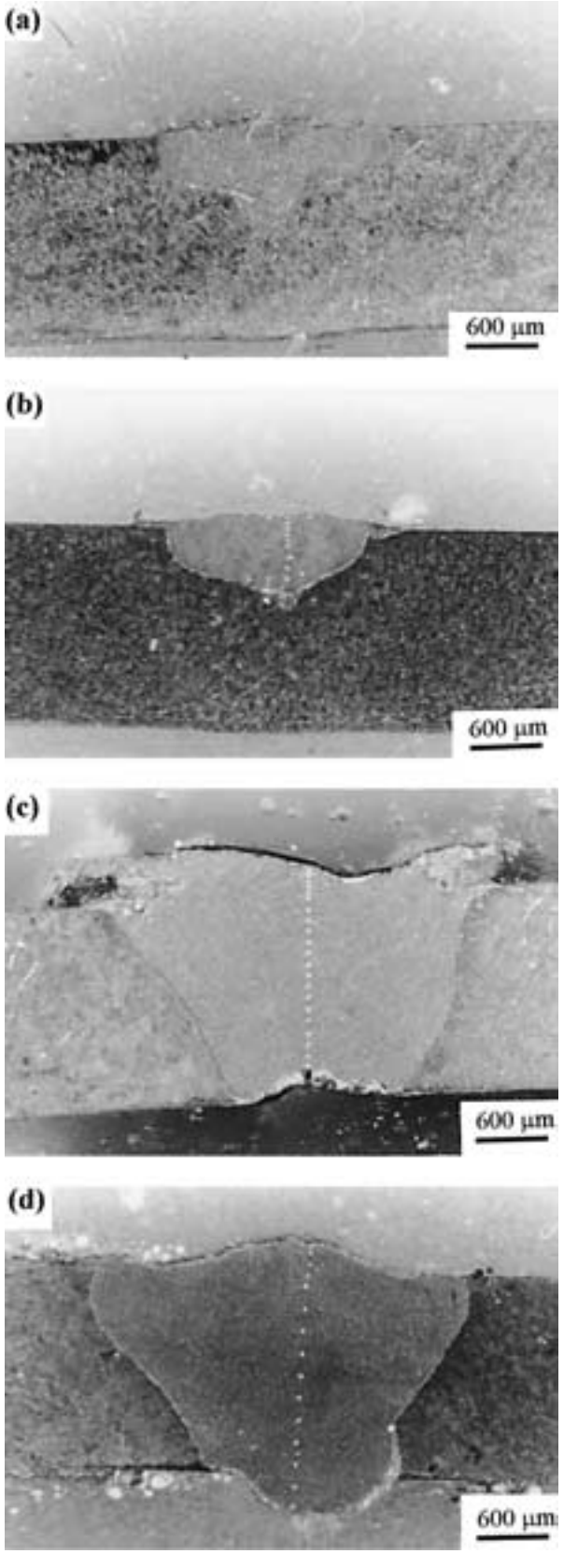

Figure 2 Melt pool configuration of laser alloyed CP-Ti with 80% Ni + 20 %SiC at power density (a) 1.3 (b) 1.9 (c) 2.5 and (d) 3.0×10^5 W cm^{-2}.

solution of carbon in titanium (TiC) a cubic phase, (b) orthorhombic titanium silicide (TiSi) and (c) hexagonal titanium silicide (Ti_5Si_3). The spectrum shows the high intensity peaks for TiC and TiSi at orientations (200) and (211), respectively. The relative XRD

TABLE II Surface condition and cracking behaviour of the LACs

Coating	Power density	Surface condition	Porosity	Cracks
80% Ni + 20% SiC	1.31×10^5 W cm^{-2}	Smooth surface	Porosity at low scan speed	No cracks inside the alloyed layer (NCIL)
60% Ni + 40% SiC	1.31×10^5 W cm^{-2}	Smooth surface	No porosity	(NCIL)
50% Ni + 50% SiC	1.31×10^5 W cm^{-2}	Rough surface at low speed, smooth surface at high speed	No porosity	(NCIL)
100% SiC	1.31×10^5 W cm^{-2}	Rough surface	No porosity	Cracks within the alloyed layer
80% Ni + 20% SiC	1.91×10^5 W cm^{-2}	rough surface at low speed and smooth surface at high speed	Root porosity No porosity	crack at the edge of the alloyed layer, NCIL crack at the surface & NCIL
60% Ni + 40% SiC	1.91×10^5 W cm^{-2}	Smooth surface	No porosity	No cracks
50% Ni + 50% SiC	1.91×10^5 W cm^{-2}	slightly smooth surface	Porosity	cracks inside the alloyed layer
100% SiC	1.91×10^5 W cm^{-2}	Rough surface	No porosity	Cracks within the alloyed layer
80% Ni + 20% SiC	$2.5–3.0 \times 10^5$ W cm^{-2}	rough surface with under cut, wide alloyed zone	No porosity	Surface cracks &
60% Ni + 40% SiC	$2.5–3.0 \times 10^5$ W cm^{-2}	rough and bulged surface with under cut, wide alloyed zone	Root Porosity	crack at the surface & (NCIL)
50% Ni + 50% SiC	$2.5–3.0 \times 10^5$ W cm^{-2}	highly rough surface, no undercut, wide alloyed zone	Porosity present	cracks inside the alloyed layer
100% SiC	$2.5–3.0 \times 10^5$ W cm^{-2}	Rough surface, no undercut, narrow alloyed zone	Porosity present	Cracks within the alloyed layer

NCIL - no cracks in the alloyed layer.

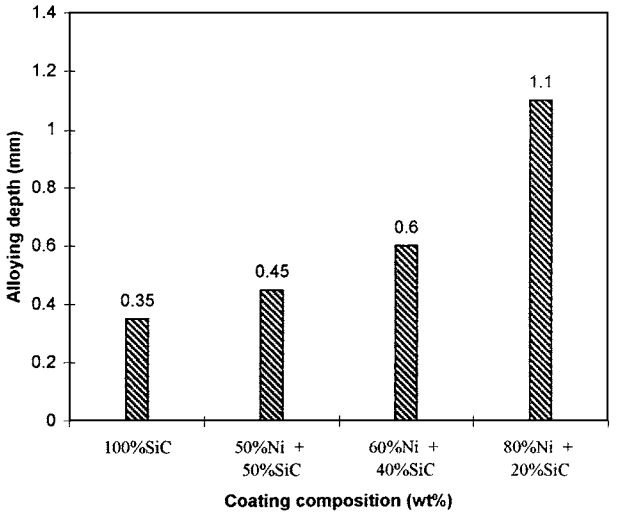

Figure 3 Effect of alloying depth as a function of nickel composition.

intensities and the calculated d-spacings of the intermetallic phases are found to be similar with ASTM values [28] indicating randomly oriented phases.

When an equal proportion of nickel and SiC (50%Ni + 50%SiC) was laser-alloyed on CP-Ti, the nickel titanium silicide (TiNiSi), titanium silicide (Ti_5Si_3) and titanium nickelide ($NiTi_2$) phases were formed on the alloyed surface (Fig. 4c). But the formation of Ti_5Si_3 was slightly stronger than the TiNiSi phase. The titanium silicide and nickelide phases formed in almost equal concentrations. The presence of $NiTi_2$ phase was relatively weaker than silicide and nickelides.

As the nickel concentration is slightly increased to 60 wt% in an Ni-SiC coating, the TiNiSi phase increased to an intense level which can be identified by the peak at (204) orientation. The XRD pattern of Fig. 4d is slightly differed from Fig. 4c. The strong intensity peaks observed at (204), (214), (018) and (136) orientations for TiNiSi suggested that this phase was formed relatively in strong level, which provides the strong evidence for the presence of TiNiSi rather than $NiTi_2$ or Ti_5Si_3. Therefore, the most dominant phase that formed during laser alloying at 60%Ni + 40% SiC condition is confirmed as TiNiSi. The presence of various intermetallic phases formed on the alloyed layer surface was attributed to the chemical reaction of the coating elements with titanium matrix and rapid solidification, which lead to non-equilibrium structure because enought time is not available for the chemical reaction to take place.

When CP-Ti was alloyed with a high nickel content of 80 wt% in a pre-placed Ni-SiC coating, the major compound phase that formed on the alloyed surface was TiNiSi. If the EDXRD pattern of Fig. 4e is compared with other diffractograms (Fig. 4b–d) it can be clearly seen that the presence of TiNiSi phase is evident by its strong peak at (204) orientation.

To analyse the compound phases formed at different coating conditions, all the XRD patterns of Fig. 4 were drafted and a comparison can be made clearly using Fig. 5. A keen observation of the XRD peaks in Fig. 5 show variations in their intensity level and revealed peak broadening. It clearly shows a large variation in the high intensity peaks. The high intensity peak of Ti

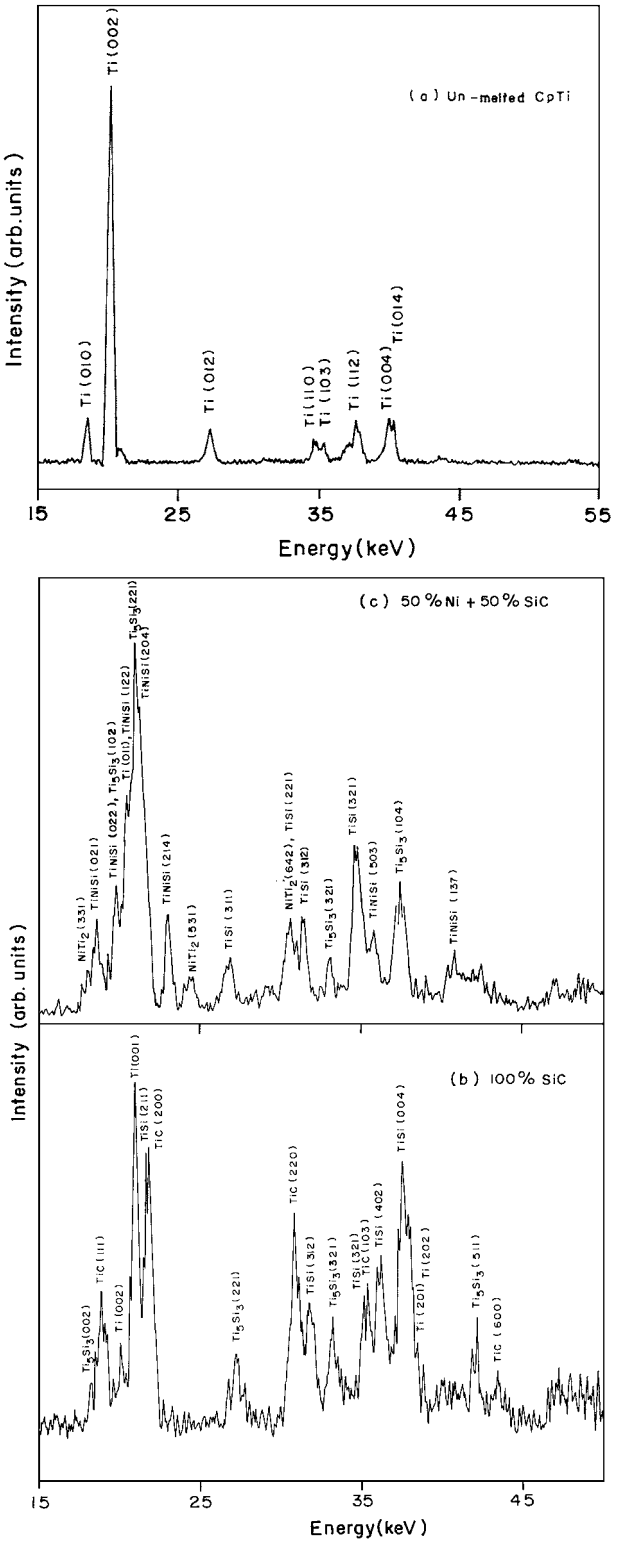

Figure 4 (a) EDXRD spectrum of unmelted CP-Ti. EDXRD spectrum of laser alloyed CP-Ti with (b) 100% SiC (c) 50%Ni + 50% SiC. EDXRD spectrum of laser alloyed CP-Ti with (d) 60%Ni + 40% SiC and (e) 80% Ni + 20% SiC.

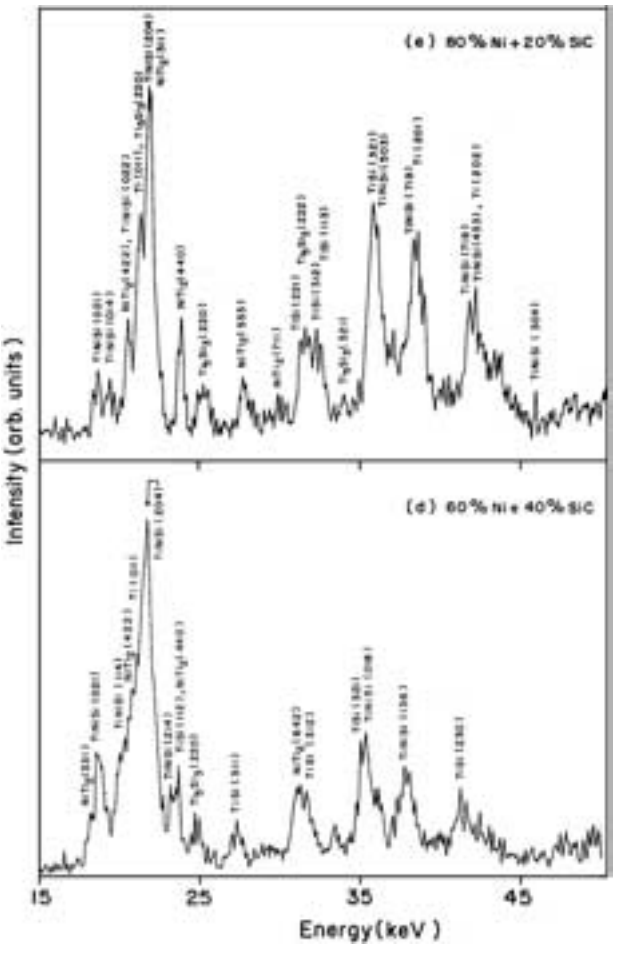

Figure 4 (*Continued*).

(001), TiSi (211) and TiC (200) at 100% SiC coating condition showed three separate peaks (Fig. 5) and it merged to become a single peak as SiC was mixed with Ni in an increasing weight percentage. In the case of 80%Ni + 20% SiC coating condition, within the 100% intensity peak there appear peak splitting with few intermetallic titanium nickelide and silicide phases. The peak splitting increases with the increase of nickel content. A comparison of all the x-ray diffractograms obtained in this study shows an interesting behaviour for TiSi at (312) oreintation. In the energy range 30–35 keV, the peaks progressively branched out and it increased with the increase of nickel content, and many phases were formed within this energy range. The same trend also appeared at the peak position present in the energy range of 35 to 39 keV. The XRD profile of the laser treated CP-Ti shows a peak broadening effect which was attributed to the development of residual stress by rapid solidification of the molten pool. The peak broadening was also attributed to the alloying effect of nickel in a Ni-SiC mixture and surface temperature.

The effect of nickel composition on the peak intensities of the TiNiSi phase at (022), (204) and (122) orientations revealed some interesting result (Fig. 6). The nickel addition with silicon carbide caused the formation of TiNiSi phase with a strong peak at (204) orientation, which found to increase with the increase of nickel content. This can be seen by comparing the peak intensities of TiNiSi phase obtained in this study with its ASTM intensity value [28].

3.5. SIMS analysis

Fig. 7 shows the results of SIMS line scan made across the laser-alloyed cross section of 60% Ni + 40% SiC coating. The profile indicates the presence of nickel (Ni), silicon (Si), carbon (C) and oxygen (O) in the α-titanium (Ti) matrix, which confirm the elements present in the preplaced coating are completely diffused

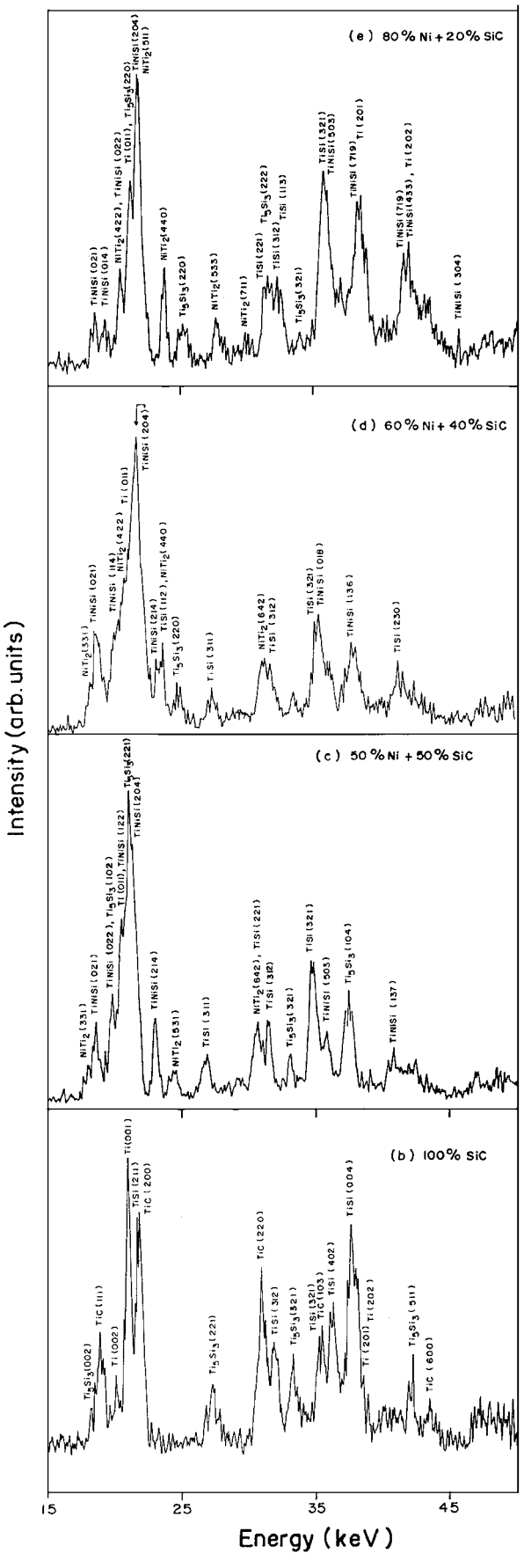

Figure 5 Comparison chart of the EDXRD spectrum for all the LACs.

into titanium during alloy formation. The elements Ni, Si and C diffused into titanium matrix can yield titanium silicide and nickelide compounds, which is also evident from EDXRD results.

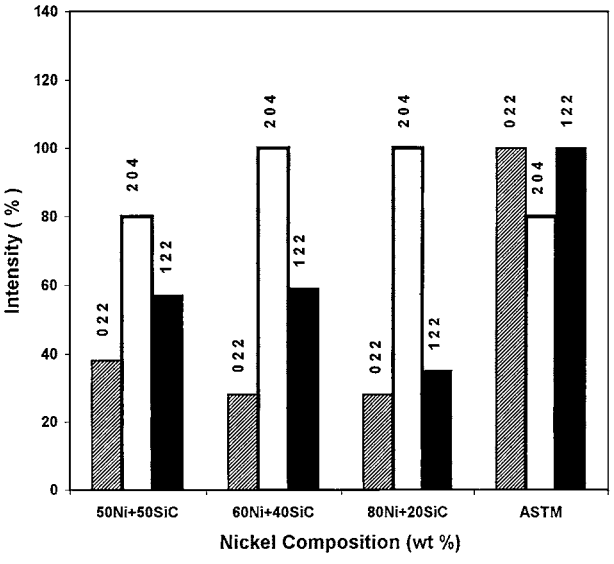

Figure 6 XRD peak intensities of the TiNiSi phase as a function of nickel composition in the laser alloyed Ni-SiC coating.

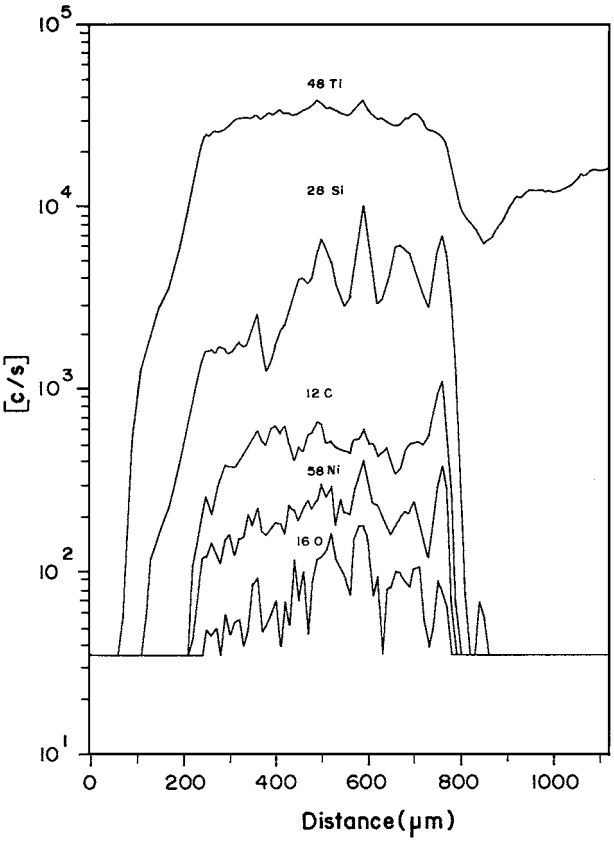

Figure 7 SIMS line scan profile showing the presence of Ni, Si, C and Ti during laser alloying of 50% Ni + 50% SiC on Ti.

3.6. Microstructural evolution

3.6.1. Effect of 80%Ni + 20% SiC coating on the microstructure formation

Fig. 8a–d shows the microstructure formed on the LAC using the pre-placed 80% Ni + 20% SiC at a power density of 1.3×10^5 W cm^{-2}. Fig. 8a shows the macrograph of the laser-alloyed zone. Fig. 8b shows the microstructure developed at the top layer of the laser-alloyed zone, consisting of nickel based intermetallic precipitates of

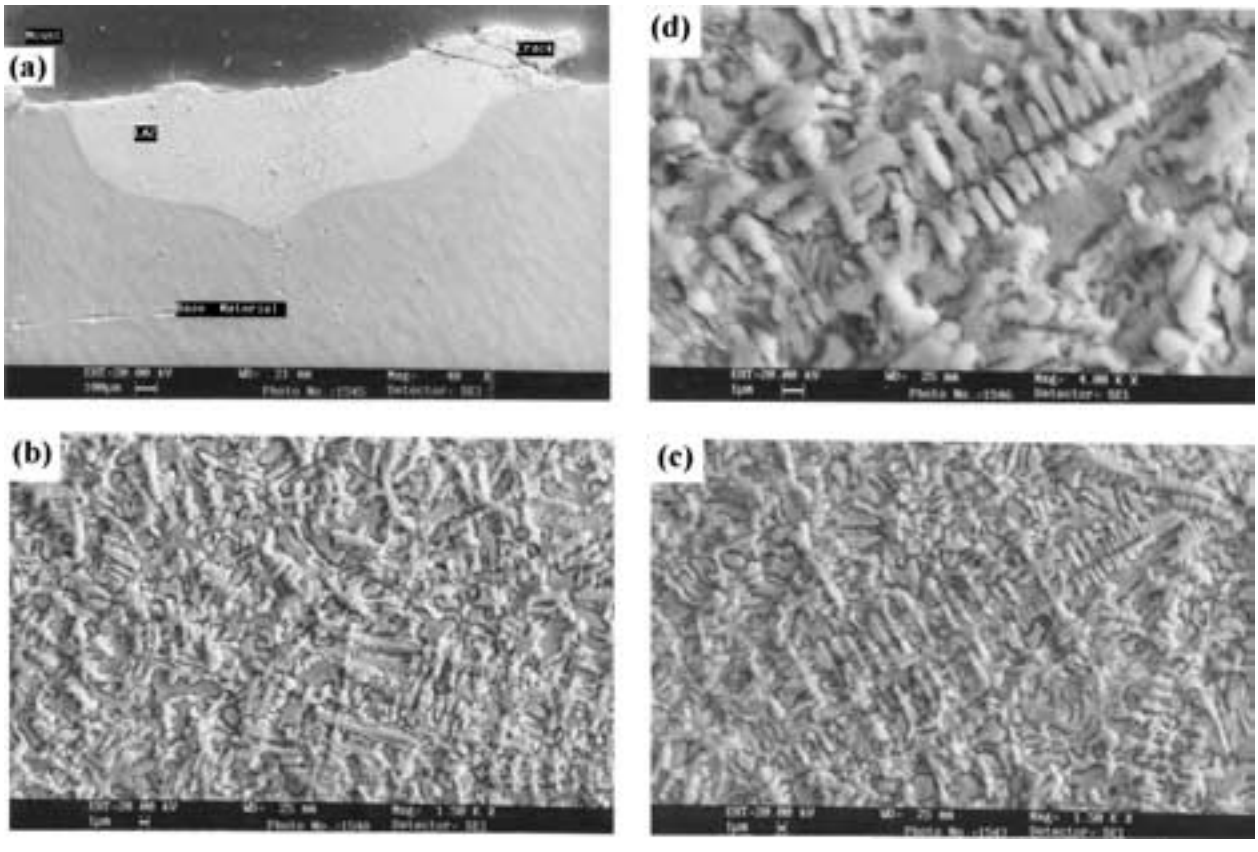

Figure 8 Microstructures of laser alloyed CP-Ti with 80%Ni + 20% SiC coating at 1.3×10^5 W cm^{-2}: (a) macrograph, (b) top region, (c) bottom region microstructure and (d) magnified view of 'c'.

dendrite and it uniformly precipitated over the entire alloyed zone. When a high nickel content of 80% Ni was added with 20% SiC and laser-alloyed on the surface of CP-Ti, the intermetallic precipitate formation seems to be high (Fig. 8b). Even in the bottom layer of the laser-alloyed zone (Fig. 8c), the density level of intermetallic precipitate (nickelides and silicides of titanium) formation is quite high and its population level is closely comparable with those formed in the top layer. Fig. 8c shows the bottom layer (slightly above the transition region) microstructure, which consisting of larger size dendrite of length 60 μm with a secondary dendrite arm spacing of 0.5 to 1 μm. Fig. 8d is the magnified view of a dendrite seen in Fig. 8c in which the measured dendrite tip radius was approximately one microns.

Fig. 9a shows the SEM macrograph of the laser-alloyed layer at 1.91×10^5 W cm^{-2}. When the power density increases from 1.3 to 1.91×10^5 W cm^{-2} porosity was developed near the transition zone. With the increase of laser power density, the density level of dendrite formation seems to increase to a certain extent (Fig. 9b). These dendrite precipitation could be the compounds of nickelide and silicides of titanium. The microstructures seen in Fig. 9c and d are the magnified view of a portion of Fig. 9b. With the increase of laser power density the dendrite length was found decreased to about 15 μm. The dendrites were found to be grown from the surface and its nucleation direction is towards the depth of the alloyed region. The dendrite seen in Fig. 9d is of lotus flower like appearance and the secondary dendrite were found to grown in radial direction.

3.6.2. Effect of 60% Ni + 40% SiC coating on the microstructure formation behaviour

Figs 10a–d and 11a–d shows the microstructure images formed during laser alloying of 60% Ni + 40% SiC coating on CP-Ti under a laser power density of 1.3×10^5 W cm^{-2} and 1.91×10^5 W cm^{-2}, respectively. When the nickel content was slightly reduced to 60% Ni in a Ni-SiC coating, the microstructures were formed in a different way. In this processing condition, the laser-alloyed cross section was found to be perfectly flat without any cracks or porosity (Fig. 10a). Fig. 10b and c show the microstructures formed at the top (50–100 μm) and central (100–150 μm) regions of the laser-alloyed layer, respectively. At this coating condition the LAC consists of fine intermetallic precipitates of dendrites. This microstructural feature of uniform intermetallic precipitation was found over the entire alloyed region. Fig. 10d is the magnified view (10,000×) of a dendrite. The measured dendrite arm spacing of 300 nm, is due to the very high cooling rate (10^6–10^8 K s^{-1}).

When the power density was increased to 1.91×10^5 W cm^{-2}, the dendrites were formed uniformly on the top and central layers (Fig. 11b–c) and the intensity level of precipitation was seen to be quite

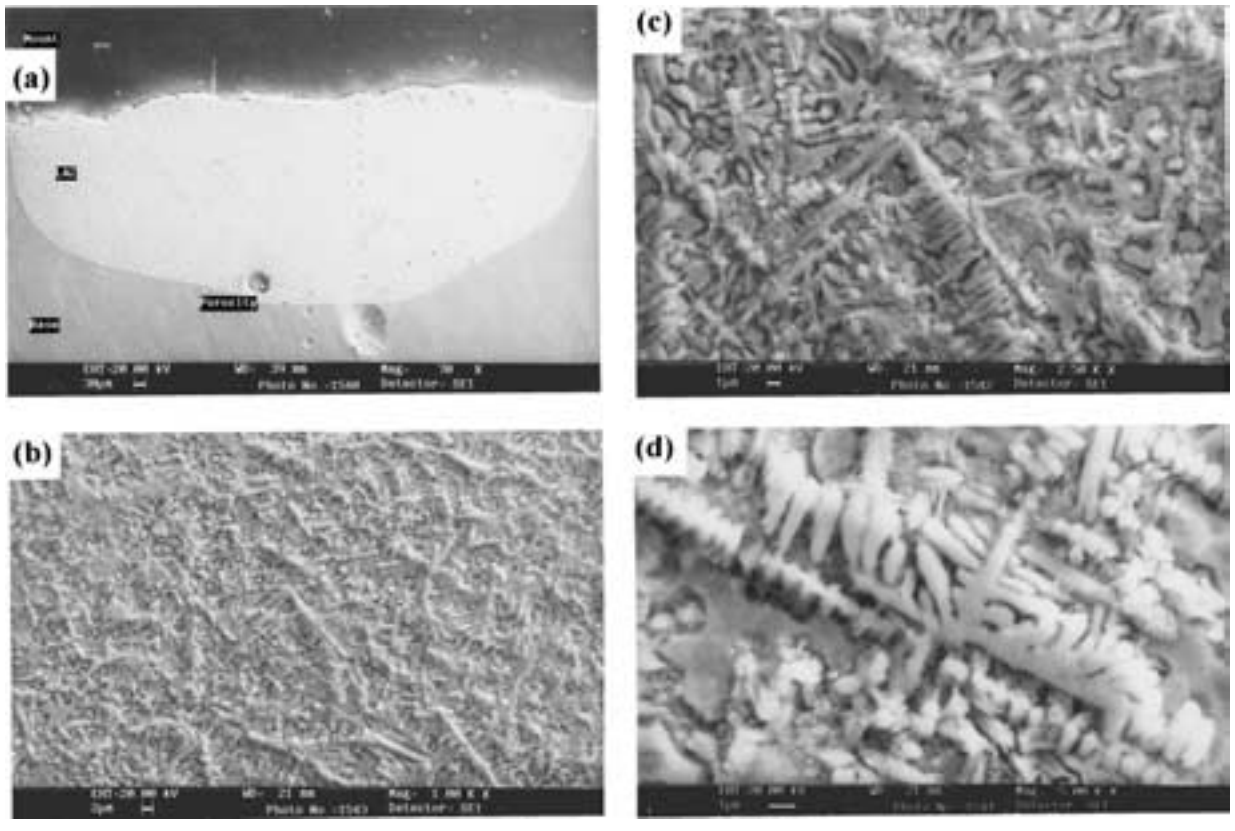

Figure 9 Microstructures of laser alloyed CP-Ti with 80%Ni + 20% SiC coating at 1.9×10^5 W cm^{-2}: (a) macrograph, (b) uniformly precipitated dendrites and (c) and (d) magnified view of 'b'.

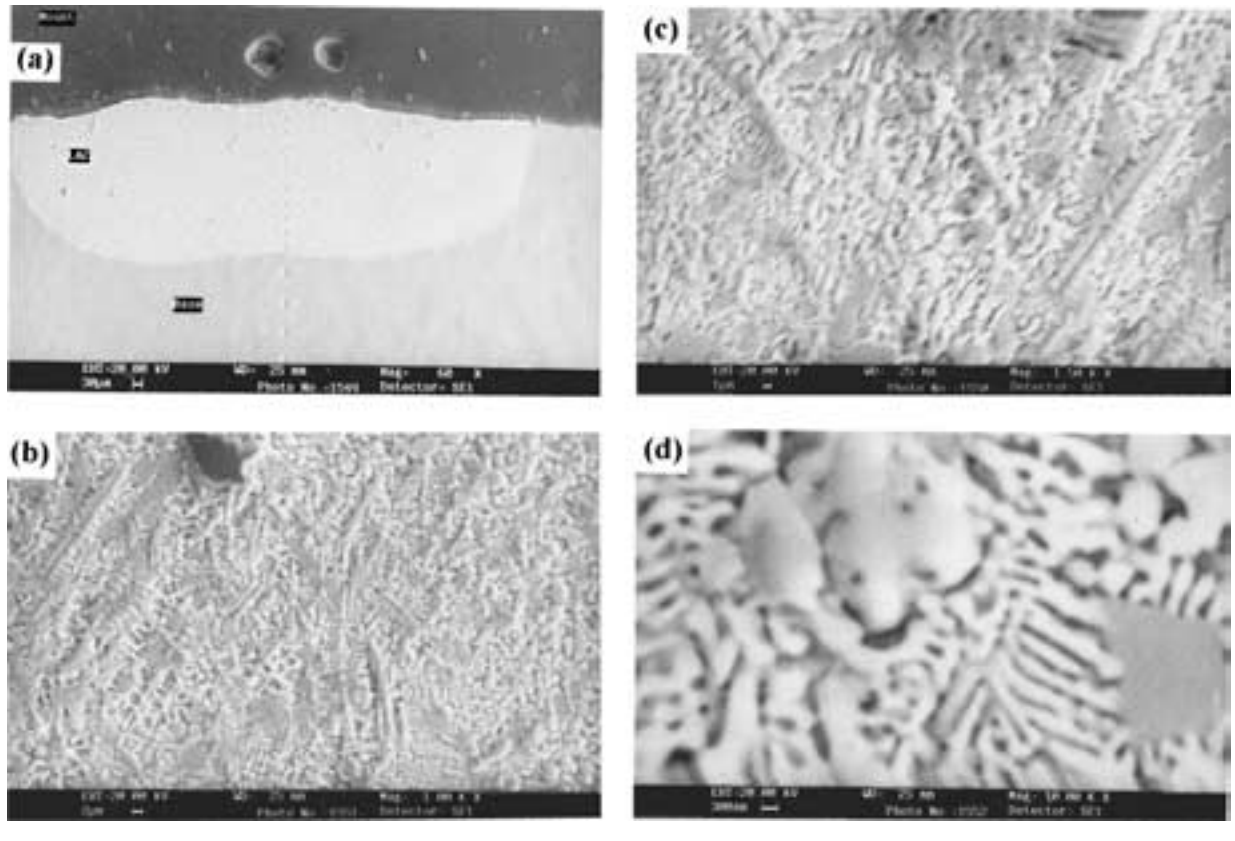

Figure 10 Microstructures of laser alloyed CP-Ti with 60%Ni + 40% SiC coating at 1.3×10^5 W cm^{-2}: (a) macrograph (b) top region (50–100 μm), (c) central region (100–150 μm) and (d) view of a dendrite at 10,000× magnification.

high. At this high power density, the increase of heat input raises the alloying temperature, which enhanced the dendrite population level. This type of microstructure increased the hardness to about 1000 HV and therefore this microstructural behaviour can improve the surface property of titanium. Near the transition region the intensity of the dendrite precipitates decreased comparatively to a low level (Fig. 10d).

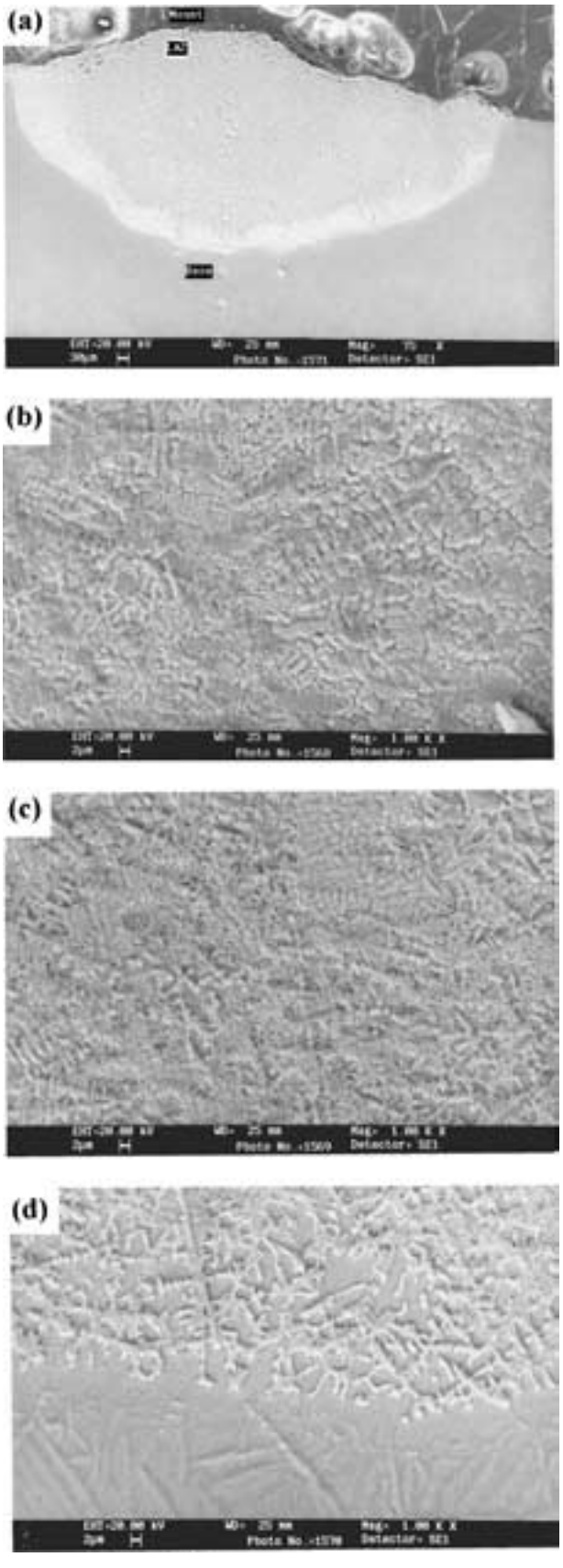

Figure 11 Microstructures of laser alloyed CP-Ti with 60%Ni + 40% SiC coating at 1.9×10^5 W cm^{-2} (a) macrograph (b) top region (50–100 μm), (c) central region and (d) transition region.

3.6.3. Effect of 50% Ni + 50% SiC coating on the microstructure formation behaviour

When a coating containing equal proportions of Ni and SiC i.e. 50% Ni + 50% SiC was laser-alloyed on CP-Ti at a power density 1.3×10^5 W cm^{-2} under a scan speed 1.0 m min^{-1}, very fine microstructure of finely distributed intermetallic nickel precipitates were resulted (Fig. 12a). The uniform dispersion of such intermetallic nickel precipitate in an alloyed coating was considered to result from the proper mixing and reaction between the completely dissolved SiC and Ni with molten titanium. This microstructure development can provide uniform hardness behaviour throughout the alloyed layer and a hardness of 900 HV was observed. The population level of the precipitates seen in Fig. 12b is larger than that occurred in Fig. 12c.

The SEM macrograph of Fig. 13a shows root porosity at the far edge of the alloyed zone. The population of the dendrites appeared to be small at the top (Fig. 13b) and bottom regions (Fig. 13c). The dendrite population was much lower than that observed at other coating conditions. This is attributed to low volume of silicon diffusion in the alloyed region. During laser alloying at a high power density of 1.91×10^5 W cm^{-2} under low scan speed 0.5 m min^{-1}, a very high-temperature of 3000–3500 °C was created at the surface. At such a high-temperature, the nickel and SiC in the pre-placed coating will completely melt and react with molten titanium to form a complete dendrite microstructure (Fig. 13a–c).

The high magnification photograph of dendrite morphology observed at the top and bottom regions of the LAC at a power density 1.91×10^5 W cm^{-2} is shown in Fig. 14a and b, respectively. The secondary dendrite arm spacing measured at the top and bottom region was about 0.25 to 2 μm. In the laser alloying process, the heating and cooling rate is faster (in the order of 10^6–10^8 K s^{-1}) because laser heating happened in a very low solidification time of 0.12 seconds. This may be the reason for the growth of dendrites with a very small secondary arm spacing.

3.6.4. Effect of 100% SiC coating on the microstructure formation behaviour

By laser alloying 100% SiC on titanium, the microstructure completely consists of the dendrite type surface morphology and their density level depends upon the laser processing condition used. Fig. 15a and b shows the optical macrograph and top region microstructures, respectively and it was obtained at low power density 1.3×10^5 W cm^{-2} under a scan speed of 1.0 m min^{-1}. Fine dendrites were uniformly distributed throughout the alloyed layer (Fig. 15a). Cracks were also observed in this layer. Very fine and dense dendrites were observed at the top region (Fig. 15b). The measured hardness at fine dendrites was about 950 HV. The dendrites were found to grow towards the matrix. At the surface, the length of dendrites was 60 μm with an arm length of 20 μm. As the power density increases (1.91×10^5 W cm^{-2}), the dendrites length seems to increase to 120–150 μm and 60–400 μm at the top and central region, respectively (Fig. 15c and d). The hardness varies according to the dendrite's length and its density level. The average hardness measured at the top and central region was 1000 HV and 600 HV, respectively.

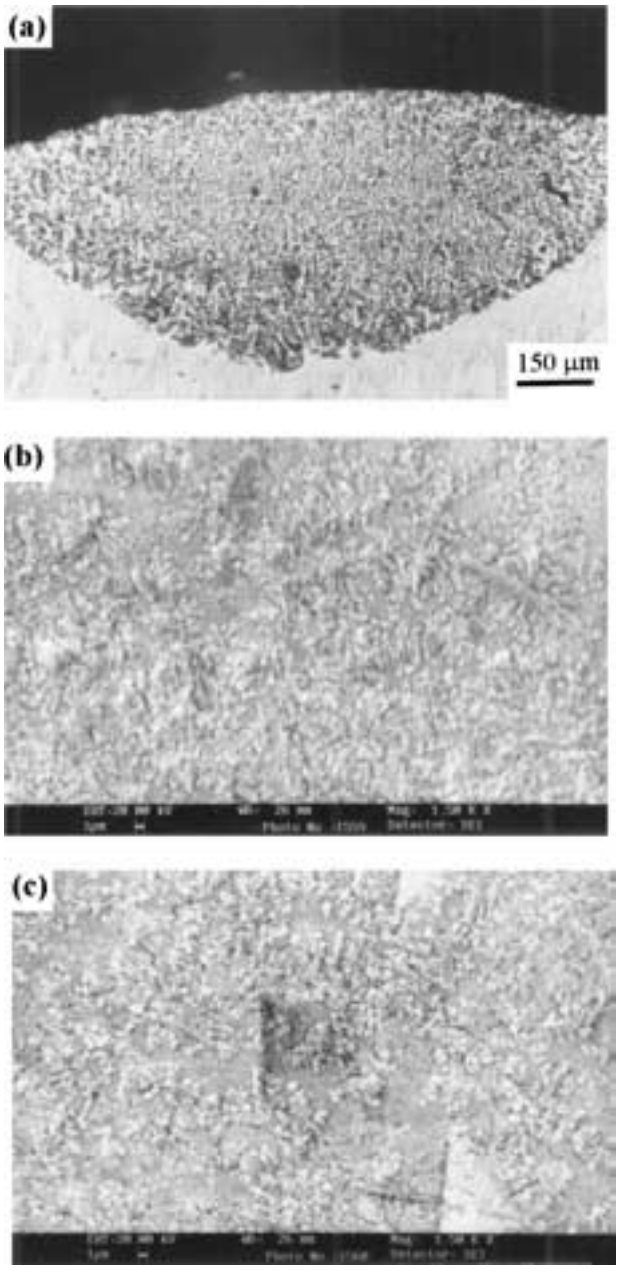

Figure 12 Microstructures obtained by laser alloying 50% Ni + 50% SiC on titanium at 1.3×10^5 W cm^{-2} (a) Optical macrograph showing titanium nickel silicide precipitates, (b) Ni precipitates at the top region, (c) SEM image of central region of Figure (a).

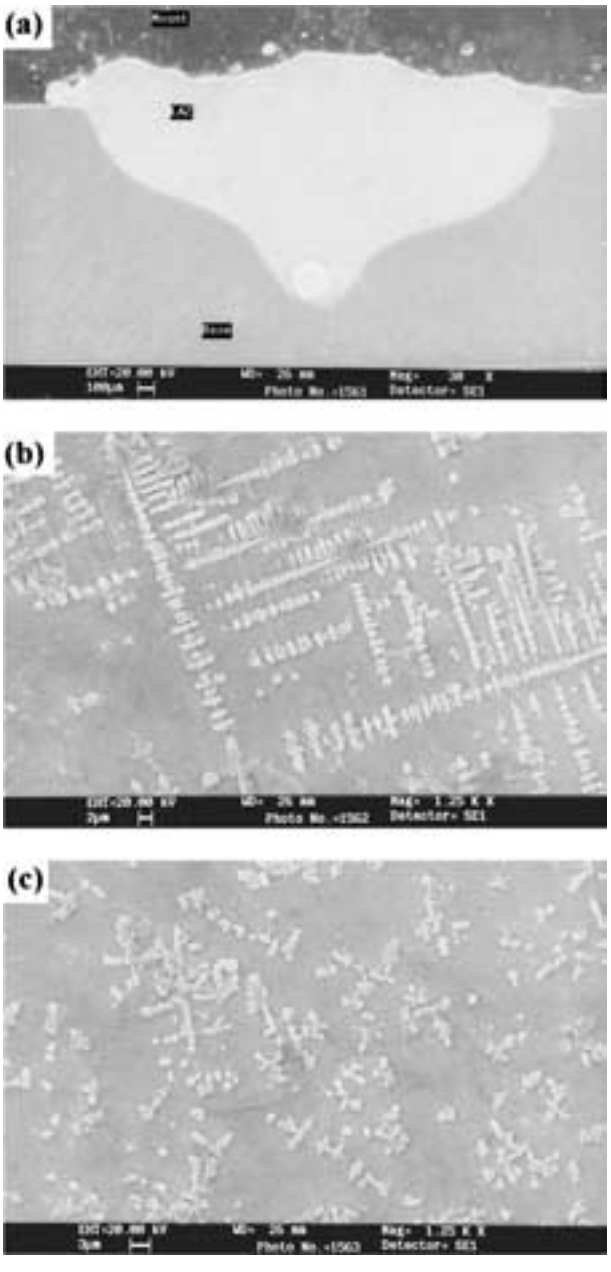

Figure 13 Microstructures obtained by laser alloying 50% Ni + 50% SiC on titanium at 1.91×10^5 W cm^2 (a) SEM macrograph showing porosity, (b) larger size dendrites at the top region, (c) smaller size dendrites at the bottom region.

The microstructures developed on the laser-alloyed surface of CP-Ti using 100% SiC at a power density 1.91×10^5 W cm^{-2} under a scan speed of 1.0 m min^{-1} are shown in Fig. 16a–e. Fig. 16a shows the SEM macrograph. The crack developed in the laser-alloyed layer is clearly visible from the magnified view of the macrograph (Fig. 16b). The crack originated from the surface was propagated throughout the alloyed layer and terminated at the transition region. When the power density increased to 1.91×10^5 W cm^{-2}, there appeared fine and intense dendrites and this can increase the hardness. When 100% SiC coating was laser alloyed on Ti, at this high laser power density, the dendrite population level is very high and the length of the dendrite become increased at the top layer (Fig. 15c). At the bottom region the density of dendrite precipitation was found decreased (Fig. 16d), because the diffusion of silicon in the alloyed layer is decreased to a comparatively low level at greater alloying depths. If the dendrites precipitated at the top region (Fig. 16c) and bottom region (Fig. 16d) are compared, it is clearly seen that the dendrite arm spacing of 1–2 μm observed in the top region increased to $\cong$10 μm at the bottom region. This indicates that the secondary arm spacing increases with the increase of alloying layer depth. The growth of smaller dendrite arm spacing at the top layer can be attributed to the high level silicon diffusion and faster reaction rate between the diffused silicon with titanium. The reaction of silicon and carbon with titanium was higher at the top region than in the bottom region and this might have contributed high level dendrite precipitation in the top layer.

Fig. 16e is the magnified view of the dendrites observed in Fig. 16c. The dendrites were nucleated in a parallel array and they were not spaced equally. The distance between the dendrite seems to increase

progressively from the left of this micrograph. This may be due to the directional solidification effect and large thermal gradient that exist within the re-solidified layer.

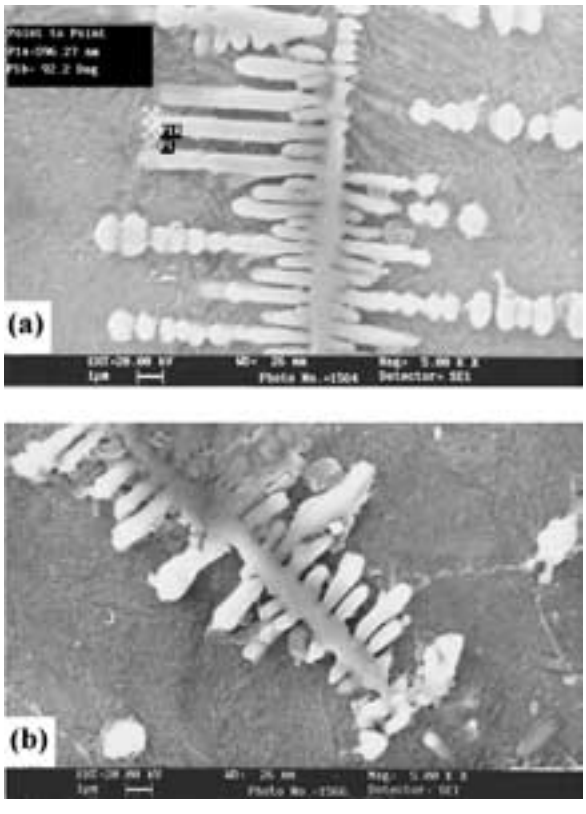

Figure 14 The high magnification of dendritic morphology observed at (a) the bottom region and (b) bottom region.

3.7. Hardness behaviour

3.7.1. Effect of low power density (1.3×10^5 W cm^{-2}) on the hardness behaviour of LAC

The hardness profiles of laser alloyed CP-Ti with 100% SiC, 50% Ni + 50% SiC, 60% Ni + 40% SiC and 80% Ni + 20% SiC coatings at laser power density 1.3×10^5 W cm^{-2} are shown in Fig. 17a–d, respectively.

When a pre-placed layer of 100% SiC was laser alloyed on CP-Ti (at low power density of 1.3×10^5 W cm^{-2} under a low scan speed 0.5 m min^{-1}) a constant hardness of 900 HV was obtained throughout the alloyed region of 400 μm thickness. It was attributed to the homogeneously distributed dendrites. At a high scan speed 1.0 m min^{-1} the high hardness 1200 HV measured at 50 μm decreased to 775 HV at a depth of 150 μm. It increased to 950 HV at 200 μm depth, then gradually decreased and reached the matrix hardness of 200 HV at a depth of 400 μm. The high hardness 1050–1250 HV observed at 50–100 μm depth is due to the undissolved SiC particles and fine dendrites. At a very high scan speed 1.5 m min^{-1}, the hardness 850 HV observed near the surface begins to decrease gradually and attains the matrix hardness at 300 μm depth.

When an equal proportion of Ni and SiC i.e., 50% Ni + 50% SiC was alloyed on CP-Ti (at a low power density 1.30×10^5 W cm^{-2}) the hardness behaves in a different way. In this case no large scale fluctuation in the hardness was observed at all the three scan speed levels. An almost constant hardness was obtained in the alloyed region (Fig. 17b). The average hardness

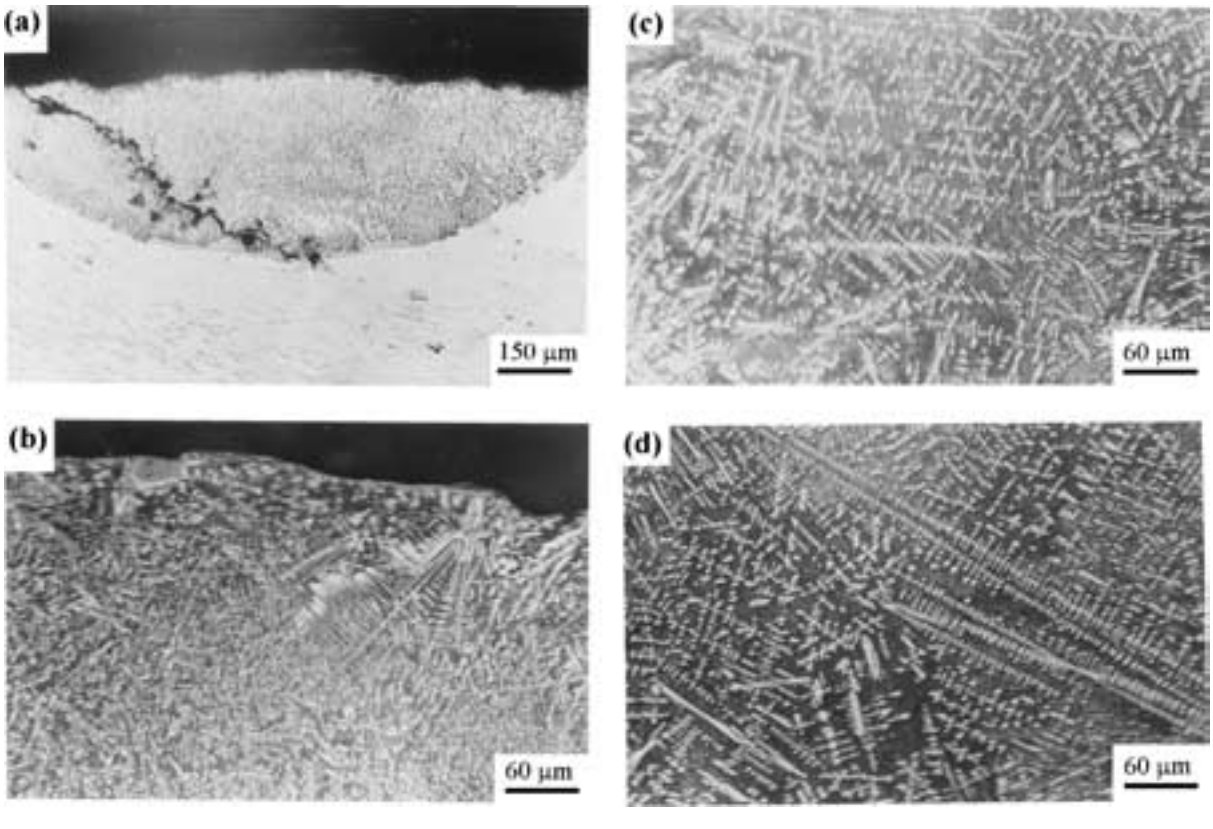

Figure 15 Optical microstructures of the laser alloyed zone at 100% SiC coating at (a) and (b) 1.3×10^5 W cm^{-2} and (c) and (d) 1.91×10^5 W cm^{-2}: (a) Optical macrograph (b) fine dendrites-top region (c) small size dendrites-top region (d) large size dendrites-central region.

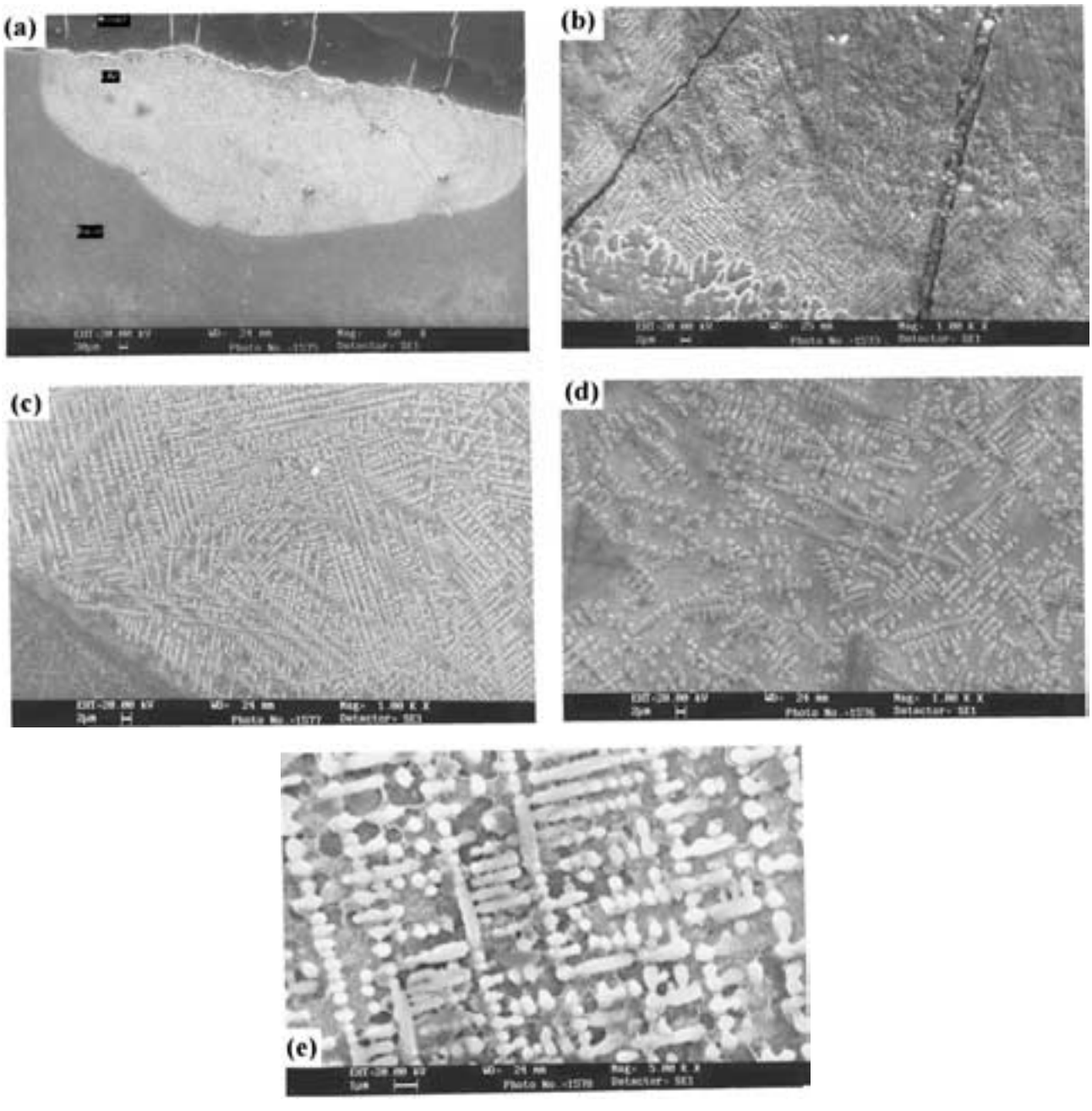

Figure 16 SEM images of the laser alloyed zone at 100% SiC coating at 1.91×10^5 W cm^{-2}: (a) macrograph (b) cracking inside the alloyed layer (c) highly populated dendrites-top region (d) low volume dendrite precipitates-bottom region (e) columnar dendrites.

measured at scan speeds of 0.5, 1.0 and 1.5 m min^{-1} were in the range of 700–800, 850–1000 and 800–1000 HV, respectively. It can be considered that when SiC and Ni were taken in equal proportions and laser alloyed, homogeneously precipitated titanium nickelide and silicide phases of titanium has given a uniform and homogeneous alloyed layer.

When the nickel content was slightly increased to 60% (in a Ni-SiC coating), the hardness maintains a constant value at low scan speed level and was found to be within the range 900 to 1000 HV (Fig. 17c). But at higher scan speed levels, the hardness decreased to 600–800 HV. When the nickel content was greatly increased to 80%, very little fluctuations in the hardness behaviour was noticed and in this case the measured hardness was 600 to 800 HV. The advantage of laser alloying of CP-Ti with a high nickel content is the formation of a larger coating thickness (Fig. 17d).

3.7.2. Effect of medium power density (1.91×10^5 W cm^{-2}) on the hardness behaviour of LAC

The micro-hardness behaviour of the laser-alloyed surface using the pre-placed layers of 100% SiC, 50% Ni + 50% SiC, 60% Ni + 40% SiC and 80% Ni + 20% SiC at medium power density 1.91×10^5 W cm^{-2} are shown in Fig. 18a–d, respectively.

When 100% SiC layer was laser alloyed on CP-Ti (at laser power density of 1.91×10^5 W cm^{-2} under scan speeds 0.5 and 1.0 m min^{-1}) a large fluctuation in the hardness was noticed (Fig. 18a), which found

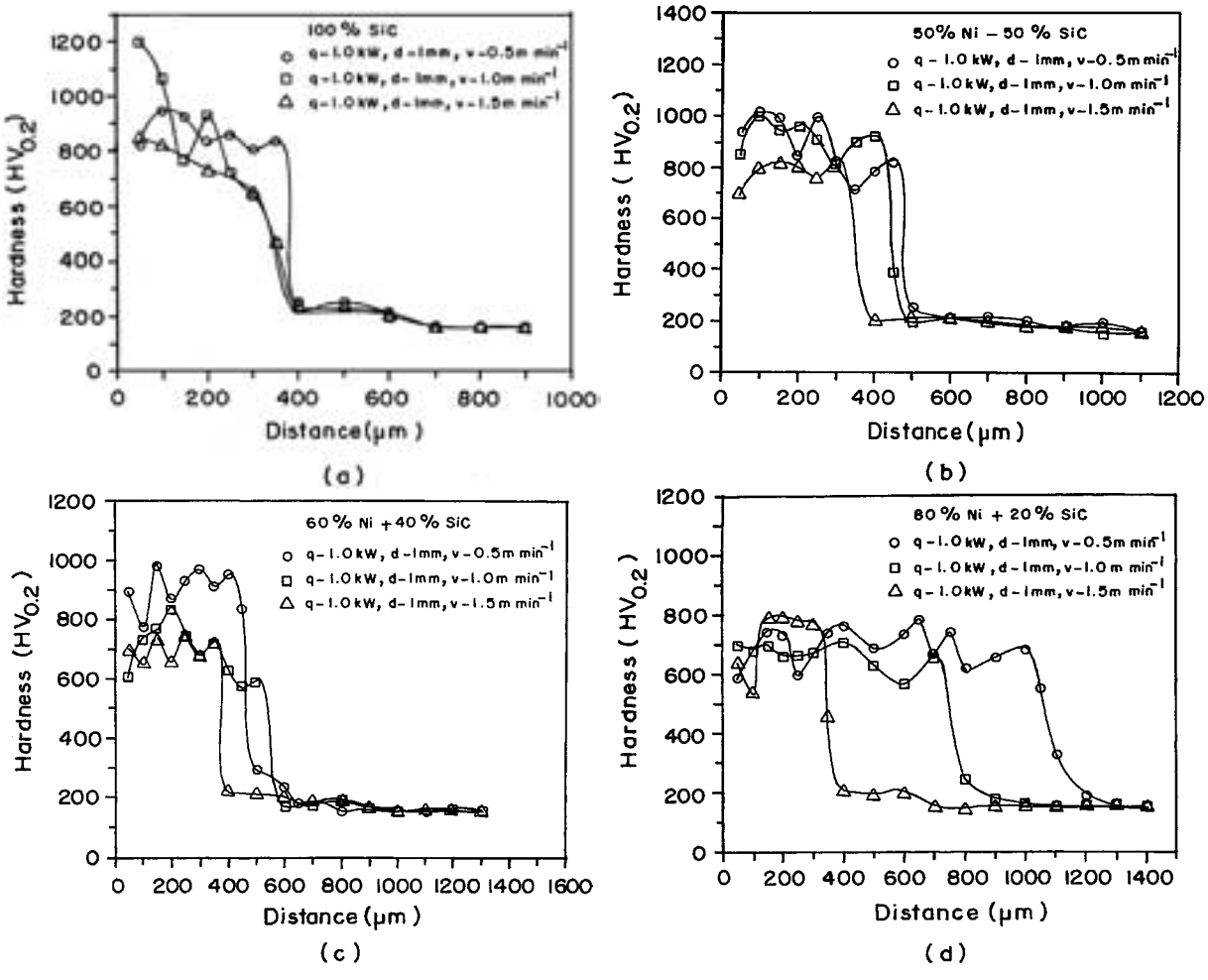

Figure 17 Hardness profile of laser alloyed CP-Ti with pre-placed coatings of (a)100% SiC, (b) 50% Ni + 50% SiC, (c) 60% Ni + 40% SiC and (d) 80% Ni + 20% SiC at laser power density 1.3×10^5 W cm^{-2}.

to vary between 500 and 1000 HV. The large fluctuation in the hardness profile at this high power density was attributed to variations in the dendrite density level. Whereas, the LAC using 50% Ni + 50% SiC (under a high scan speed 1.0 m min^{-1}) produced a constant hardness behaviour throughout the alloyed coating and it was found to be about 900 HV (Fig. 18b). When processing was carried out at low scan speed 0.5 m min^{-1}, due to high processing temperature the hardness drastically reduced to 550 HV, which is maintained throughout the alloyed layer depth of 1600 μm. At this processing condition (1.91×10^5 W cm^{-2} under a low scan speed of 0.5 m min^{-1}) the surface temperature exceeds the boiling point of titanium, which softens the alloyed layer and reduced the hardness drastically to a low value of 500 HV. As the nickel content was slightly increased to 60% (in a Ni-SiC coating), a uniform level of hardness within the range of 800–1000 HV was obtained at both the scan speeds (Fig. 18c). In the case of very high nickel content i.e. 80% Ni + 20% SiC coating condition, fluctuations in the hardness behaviour was noticed but it was considerably lower and it was found to be lower than that obtained at 100% SiC coating condition. In this case, the hardness range measured at low and high scan speed levels were 700–1300 and 450–800 HV, respectively. Peak hardness of 1300 HV was observed at a far depth of 450 μm and it was due to the undissolved SiC particles dispersed in the titanium matrix. At this processing condition a larger hardened depth was obtained.

3.7.3. Effect of very high power density (2.5 and 3.0×10^5 W cm^{-2}) on the hardness behaviour of LAC

At very high laser power density 2.5 and 3.0×10^5 W cm^{-2}, the hardness behaviour of LACs using the pre-placed layers of 100% SiC, 50% Ni + 50% SiC, 60% Ni + 40% SiC and 80% Ni +20% SiC are shown in Fig. 19a–d, respectively. At very high power densities the LACs resulted in large hardness fluctuations for all the coating conditions irrespective of the pre-placed SiC or Ni-SiC. In all the pre-placed coating conditions the hardness declined to about 500 HV. At higher power density, high-temperature developed at the coating surface initiates a keyhole and due to this most of the incident laser light was absorbed by the coating. In this situation, the high-temperature liquid melt pool resulted in large convective flow, which increased the alloying depth to a greater extent. At a high-temperature range of 3700–4900°C, a partial amount of the metallic elements in the pre-placed coatings was vaporised. Hence a low volume of nickel

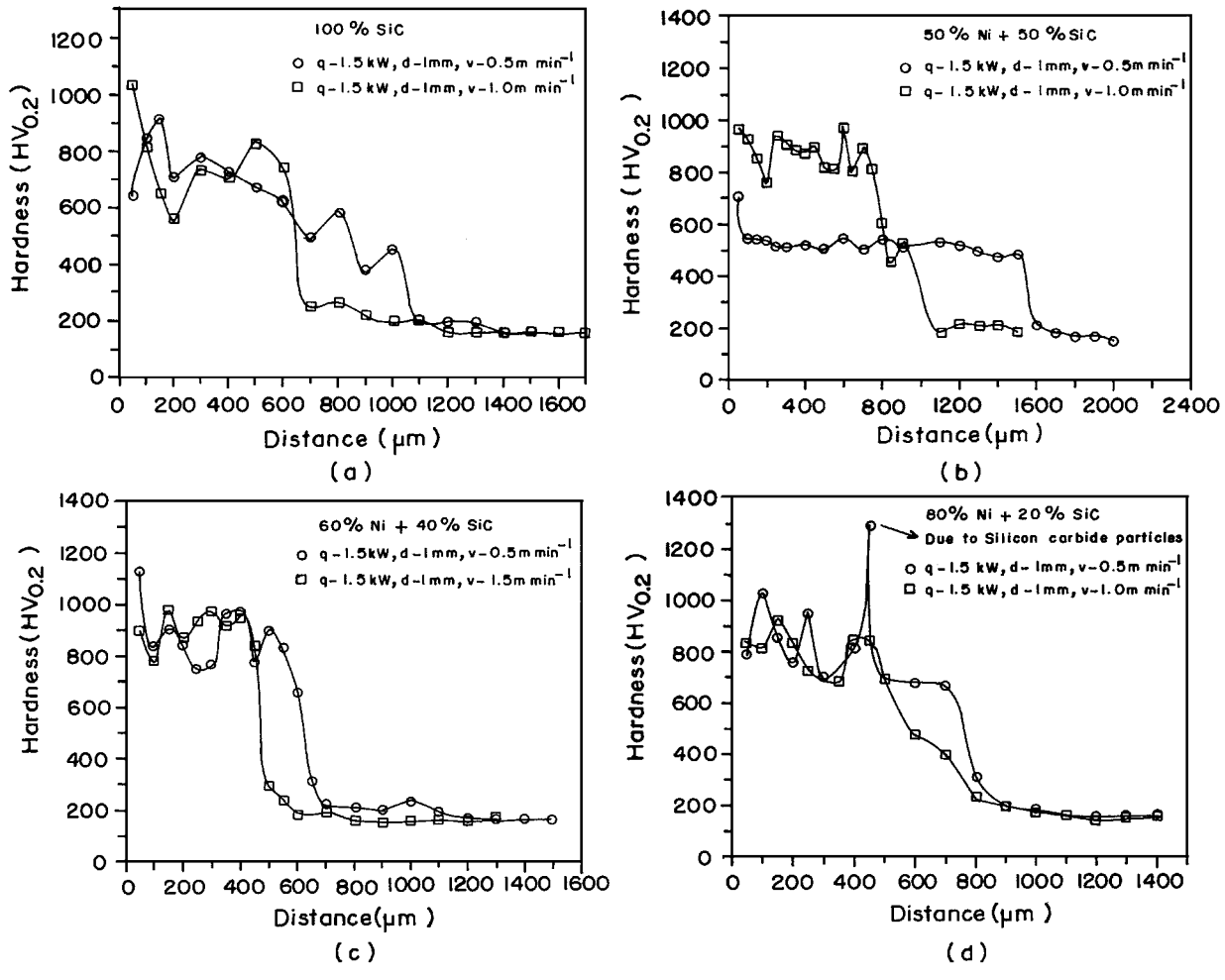

Figure 18 Hardness behaviour of the laser alloyed surface using pre-placed coatings of (a) 100% SiC, (b) 50% Ni + 50% SiC, (c) 60% Ni + 40% SiC and (d) 80% Ni + 20% SiC coatings at medium power density 1.91×10^5 W cm^{-2}.

and silicon were dissolved into the molten pool of titanium, which decreased the hardness value to about 500 HV.

By comparing the hardness profiles of all the LACs shown in Figs 17 to 19, it was found that the low level laser power density of 1.31×10^5 W cm^{-2} seems to be highly efficient for producing a homogenous and uniform hardened layer with an appreciable alloying depth of 0.4–0.6 mm. The medium level laser power density of 1.91×10^5 W cm^{-2} may also be used for producing a homogeneous alloyed layer. The high level laser power density of $2.5–3.0 \times 10^5$ W cm^{-2} was found to be inefficient for the creation of uniform alloyed layer on CP-Ti with pre-placed SiC/Ni-SiC coatings. It was found that a 50% Ni + 50% SiC coating behaves in a better way than other combinations in Ni-SiC and 100% SiC conditions. To produce a larger alloying depth, 80% Ni + 20%SiC coating may be preferred but at the expense of non-homogeneous alloyed layer.

4. Discussion

4.1. Alloying depth

It is a known fact that the laser energy absorption of a highly polished nickel surface is poor and generally very low. Whereas, coarse nickel powder with a larger particle size can improve the laser energy absorption. When coarse nickel powder mixed with SiC ceramics is used for laser alloying experiments, the laser energy absorption can be doubly increased to a high level. From the thermophysical parameters of Ni and SiC, it was seen that the thermal conductivity of nickel is higher than silicon carbide. The absorption of laser energy by nickel also seems to be high due to its high thermal conductivity value. So it can give its energy to the neighbouring SiC particles and enhance the absorption efficiency. The carbide ceramics have the greater affinity to a laser light of 10.6 μm wavelength, and as a result it can absorb most of the incident laser light. Due to this effect, a large heat energy was produced on the surface which transferred it to the surrounding nickel atoms. Therefore, nickel begins to melt instantaneously. As the melting point of silicon carbide is higher than nickel, the absorbed energy is momentarily utilised by nickel to melt. Hence, nickel particles melted completely before SiC and activate initiation of a key hole. Due to the keyhole formation most of the incident laser energy was absorbed and this has favoured a greater alloying depth. In a Ni-SiC coating, with increase in nickel percentage, the alloying depth increased due to the increase in the laser energy absorption.

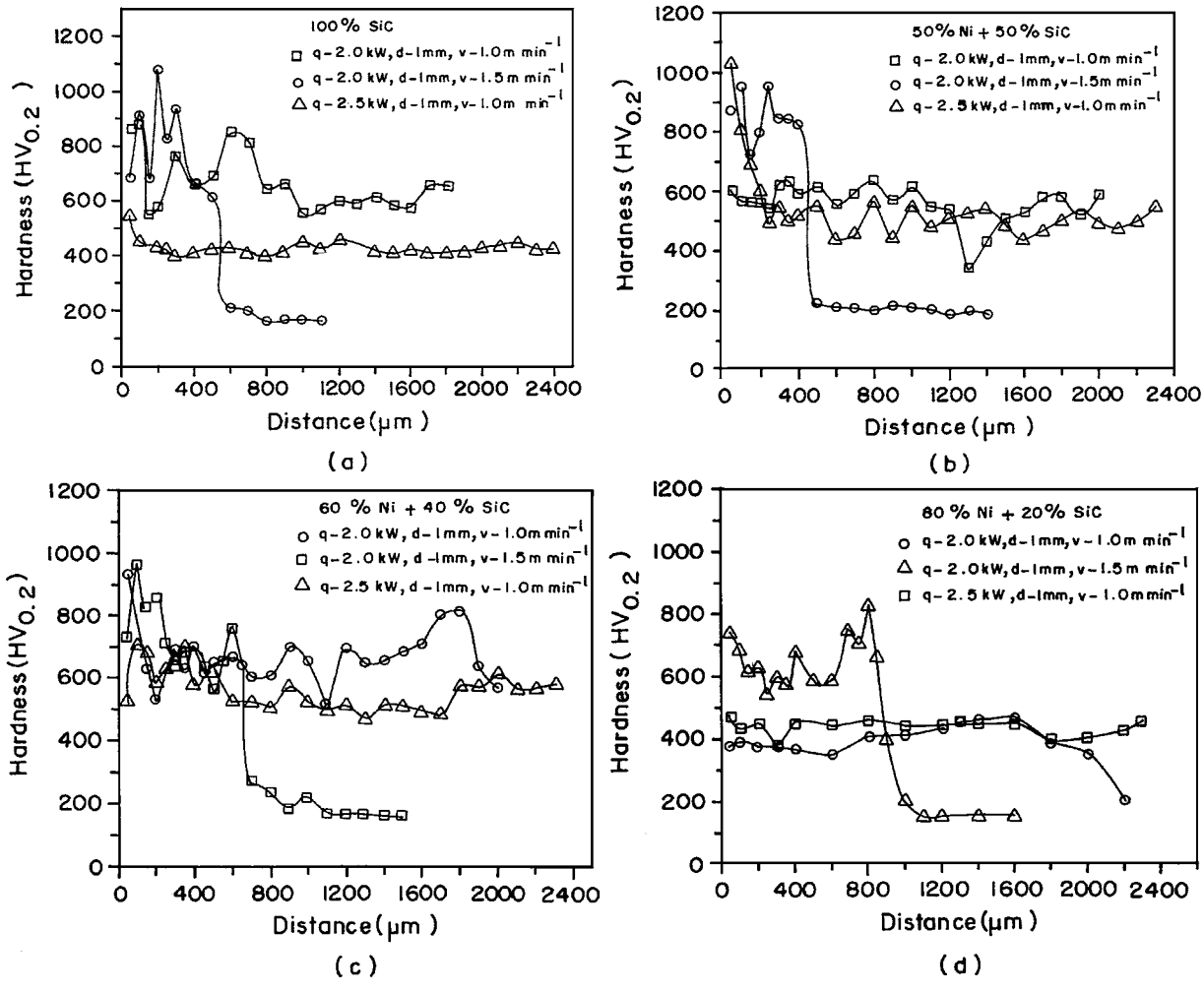

Figure 19 Hardness behaviour of laser alloyed layer at pre-placed (a) 100% SiC, (b) 50% Ni + 50% SiC, (c) 60% Ni + 40% SiC and (d) 80% Ni + 20% SiC coatings under very high laser power density 2.5 and 3.0×10^5 W cm^{-2}.

4.2. Surface temperature estimation, microstructure and compound phase formation:- A property correlation

The surface temperature estimation during laser alloying process can be useful in analysing the microstructural changes occurring in laser alloying of Ni-SiC on titanium. During a short laser interaction time the heat was diffused into titanium substrate through a thin (75–100 μm) Ni-SiC pre-placed coating. In the present context, the prediction of surface temperature for each pre-placed coating conditions are a slightly complicated process, because the composition of Ni and SiC is not constant and varies from one to other coating (i.e. 80% Ni + 20% SiC, 60% Ni + 40% SiC, 50% Ni + 50% SiC). For example, in 80% Ni + 20% SiC coating condition, the nickel concentration is high and it has been considered as a main constituent element responsible for laser energy absorption but at the same moment the role of SiC can not be eliminated. If we take 50% Ni + 50% SiC coating, the energy absorption may be equally shared by Ni and SiC. In this present situation it is difficult to estimate the surface temperature as the coating contains different compositions of nickel and silicon carbide. So, in this experiment, for the ease of analysis the surface temperature was estimated individually for Ni and SiC using the following equation [29],

$$T_o = \frac{q\eta}{r\lambda}\left[0.147 - 0.054 \ln \frac{vr}{4\alpha}\right] \quad (1)$$

where q-laser power, η-absorptivity, λ-coefficient of thermal conductivity, α-thermal diffusivity, v-travel speed and r-beam radius.

The surface temperatures estimated at various laser processing conditions for Ni and SiC were found in the range of 1500–4000°C and 1900–4900°C, respectively (Table I). From Table I, it was found that the estimated temperature values for Ni is higher than for SiC. The estimated surface temperature values at low laser power density of 1.3×10^5 W cm^{-2} was 2000–2400°C; it increases to 3000–3500°C at medium laser power density 1.91×10^5 W cm^{-2} and at high power density $2.5–3.0 \times 10^5$ W cm^{-2} it shows a very high value of 3900–4900°C. At a low power density of 1.30×10^5 W cm^{-2}, the temperature estimated for the pre-placed surface layers of Ni and SiC was 2000–2400°C. This surface temperature value is higher than the melting points of Ni and Ti, and it is very close to the melting point of SiC. At this surface temperature level, the nickel in the pre-placed coating initially

melted and transferred heat to SiC. It is thought that nickel is considered to pre-heat the SiC. Therefore SiC absorbs laser energy and beings to melt. Thus the coating elements melted and mixed with the underlying molten titanium by means of large melt pool convection velocity. Upon solidification the frozen layer by rapid cooling resulted in dendritic microstructure and nickel precipitates. The phase or crystal structure of the dendrite or other precipitates was not identified using transmission electron microscopy/selected area diffraction technique. But EDXRD analysis performed on the alloyed surface revealed the presence of nickelides and silicides of titanium and hence it can be confirmed that the dendritic morphology may consist of these (nickelides and silicides of titanium) intermetallic phases.

The microstructures resulted during laser alloying of Ni-SiC coating at different Ni and SiC compositions were mostly dendrites and the dendrite precipitation was found to increase with the increase of SiC content. It is suggested that the high nickel content (in Ni-SiC coating) seems to distort the dendrite growth and it reduces the nucleation growth rate of dendrites. When the amount of nickel in the Ni-SiC coating is decreased to about 50%, the dendrite precipitation level was found to increase and at 100% SiC coating condition the alloyed layer fully consists of dendrites. The large surface tension gradient, temperature gradient and density variations exist between SiC, Ni and Ti (Table III) and produce a strong convective flow which in turn results in inhomogeneous microstructure and fluctuations in hardness.

Due to laser heating, the pre-placed SiC dissociates into silicon and carbon [30], and in association with nickel and titanium it can form different intermetallic precipitates. The chemical reactions involved during the laser alloying process is shown in the flow chart (Fig. 20). In the case of laser alloying of CP-Ti with 100% SiC, the possible intermetallic phase formation

TABLE III Material properties of SiC, Ti and Ni

Material property	SiC	Ti	Ni
Density (gm cm^{-3})	3.217	4.507	6.908
Melting point (°C)	2200	1668	1453
Thermal conductivity ($W m^{-1} K^{-1}$)	55	16	90
Thermal diffusivity ($\times 10^{-6} m^2 s^{-1}$)	2.9	2.15	22.8
Specific heat capacity ($J Kg^{-1} C^{-1}$)		519	444
Absorptivity (at 10.6 μm)	25%	40%	30%

is generally titanium silicide and titanium carbide. According to the Ti-Si phase diagram [30] (Fig. 4), the Ti_5Si_3 phase congruently melts at a high-temperature of 2130°C and the TiSi phase melts only at 1330°C. The Ti_5Si_3 has 24.4 to 27.7 wt % silicon and TiSi phase has a high silicon content of 37.0 wt %. The formation of different titanium silicide phases indicates that the alloyed coating consists of non-equilibrium phases with varying silicon content. In addition, there exists a TiC compound phase. From the Ti-C phase diagram (Fig. 4) it was observed that the TiC phase has a high melting point of 3067°C with a carbon content of 10 to 19.3 wt %. The availability of carbon content in 80% Ni + 20% SiC may not be sufficient to form a TiC phase. But at this condition the TiNiSi phase was formed in asssociation with the Ti_5Si_3 and TiSi phases. Also the molten nickel combined with titanium forms a $NiTi_2$ phase and according to Ti-Ni phase diagram (Fig. 21) it was found that this phase has a nickel content of 38 wt%.

Thus it is found that the rapid heating and very high-temperature reached at the coating surface completely melts the metallic elements to diffuse into molten titanium. The decomposed species chemically react with base titanium and yield intermetallic phases such as titanium silicides (TiSi, Ti_5Si_3, TiNiSi), titanium nickelide ($NiTi_2$) and titanium carbide (TiC). The $NiTi_2$ intermetallic phase possesses the property of improving

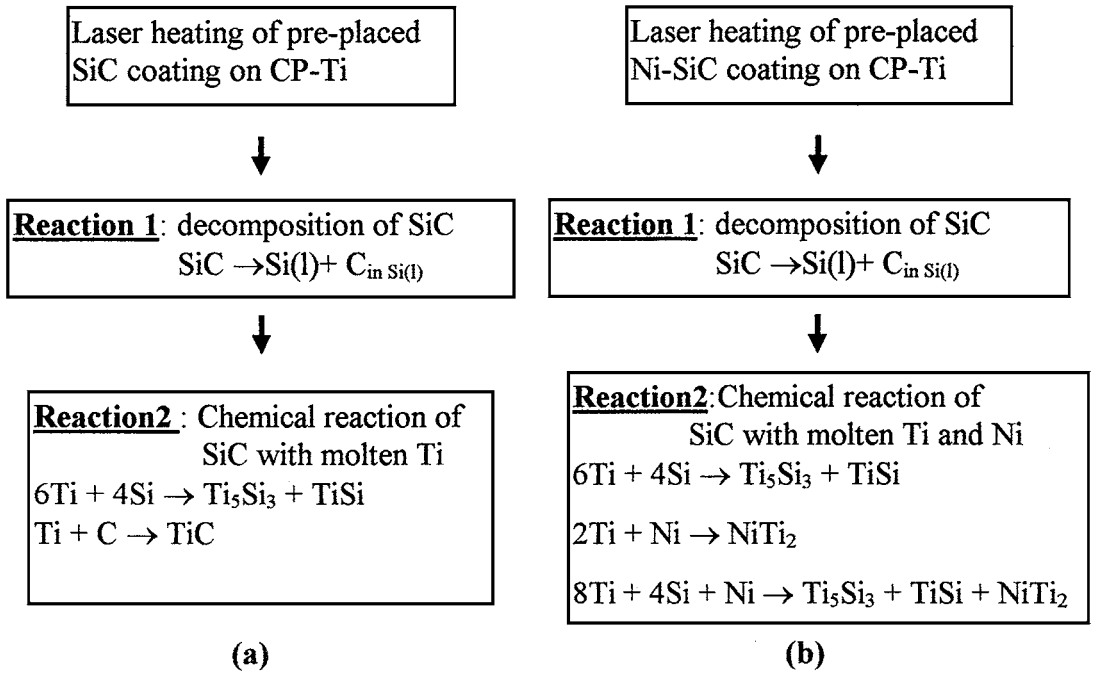

Figure 20 Flow chart showing the proposed chemical reactions during laser alloying of CP-Ti with (a) SiC (b) Ni-SiC.

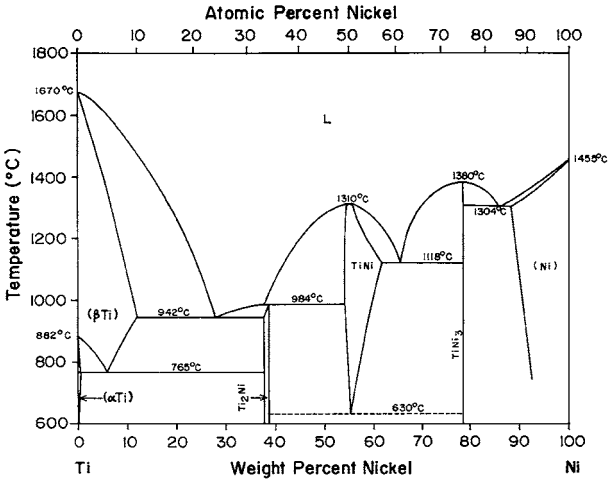

Figure 21 Binary Ti-Ni phase diagram.

the ductility and fatigue resistance [31]. In addition, the formation of other silicides of titanium such as TiSi, TiNiSi and Ti_5Si_3 was due to microstructural refinement and solid solution hardening effect [32, 33]. These are the potential strengtheners, which can improve oxidation, corrosion resistance, wear resistance and high-temperature property of titanium [34, 35].

5. Conclusion

1. High-temperature thermal barrier coating was developed on a CP-Ti surface using laser alloying technique, with Ni-SiC as the a pre-placed layer. The Ni-SiC coating with 50–60% nickel content is efficient in producing a uniform and homogeneous layer. Hence this particular composition can be adopted for creating a good thermal barrier coating.

2. The surface features of the laser-alloyed coatings at various laser variables were extensively studied with respect to cracking, porosity, and uniform surface behaviour. It was found that the laser power density of 1.3 to 1.9×10^5 W cm^{-2} (q-1.0 to 1.5 kW, d-1 mm, v-0.5 to 1.5 m min^{-1}) is efficient for producing a flawless coating with a uniform hardness level. The transverse cross section of CP-Ti alloyed with 100% SiC coating revealed extensive cracks within the alloyed zone. Cracks were scarcely found in the case of Ni-SiC coatings.

3. A uniform coating of thickness 0.4–0.6 mm was created at low power density, which may be sufficient for high-temperature applications. The coating thickness increases with increase of nickel composition. An analysis of the alloying depth at various Ni-SiC and SiC conditions suggested that the coating with a composition of 80% Ni + 20% SiC can be used for developing a thermal barrier coating with higher layer thickness.

4. The melt zone of the LAC consists of dendrite type microstructures. The degree of dendrite formation depends upon the coating composition (Ni and SiC) and laser variables. The dendrite density level was very high when a pre-placed coating of 100% SiC was utilised for laser alloying the CP-Ti. Whereas, when nickel was substituted for SiC the dendrite population level decreases and it was formed in association with nickel based intermetallic precipitates.

5. Uniform hardness was obtained for all the LACs processed under low laser power density of 1.3×10^5 W cm^{-2}. When laser alloying was carried out at a high power density of 1.91×10^5 W cm^{-2}, a uniform hardened layer was obtained for the coatings based on Ni-SiC only. At 100% SiC coating condition large fluctuations in the hardness behaviour was noticed. The use of very high power density of $2.5–3.0 \times 10^5$ W cm^{-2} is not suitable for laser alloying the CP-Ti using SiC and Ni-SiC as a pre-placed coating in which extreme fluctuations in the hardness behaviour was caused. Laser alloying of SiC and Ni-SiC on titanium has produced a composite coating with a hardness 600–1200 HV, which is three to six times higher than the base titanium. The high hardness can improve the wear resistance of titanium.

6. Laser alloying of CP-Ti with 100% SiC produced titanium silicide (Ti_5Si_3, TiSi) and carbide (TiC) phases. Whereas, laser alloying with Ni-SiC consisting of titanium silicide (TiNiSi, Ti_5Si_3, TiSi) and titanium nickelide ($NiTi_2$) phases. These intermetallic phases can improve high-temperature properties of titanium and its alloys.

Acknowledgements

The authors would like to thank Dr. A. K. Nath at CO_2 laser division, Centre for Advanced Technology in Indore, India for help during laser processing of the samples and Dr. A. K. Gogia, Scientist 'F' of Defence Metallurgical Research Laboratory at Hyderabad, India for providing CP-Ti alloy for the research work.

References

1. V. P. SWAMINATHAN and N. S. CHERUVU, "Advanced Materials and Coatings for Combustion Turbines" (ASM International, Materials Park, OH, 1994).
2. G. W. GOWARD, *Mater. Sci. Tech.* **2** (1986) 194.
3. T. N. RHYS-JONES, *Surf. and Coating Tech.* **43/44** (1990) 402.
4. F. S. PETIT and G. W. GOWARD, in "Coatings For High-temperature Applications," edited by E. Lang (Applied Science Publishers, Essex, England, 1983) p. 341.
5. R. MEVEREL, C. DURET and R. PICHOIR, *Mater. Sci. Tech.* **2** (1986) 201.
6. R. J. GILL and R. C. JR. TUCKKER, *ibid.* **2** (1986) 207.
7. A. R. NICOLL, H. GRUNER, G. WUEST and S. KELLER, *ibid.* **2** (1986) 214.
8. D. F. BETRIDGE and R. G. UBANK, *ibid.* **2** (1986) 232.
9. D. H. BOONE, *ibid.* **2** (1986) 232.
10. E. VANDEHHAR, P. A. MOLIAN and M. BALDWIN, *Surf. Eng.* **4** (1988) 159.
11. G. W. GOWARD, in "Source Book on Materials for Elevated Temperature Applications," edited by E. F. Bradley (ASM International, Materials Park, OH, 1979), p. 369.
12. P. C. FELIX, in "Materials and Coatings to Resist High-temperature Corrosion," edited by D. R. Holmes and A. Rahmel (Applied Science Publishers Ltd., Essex, England, 1978) p. 199.
13. W. BETZ, in "Materials and Coatings to Resist High-Temperature Corrosion," edited by D. R. Holmes and A. Rahmel (Applied Science Publishers Ltd., Essex, England, 1978) p. 185.
14. S. CHAKRAWARTHY, P. LI. V. TIRABASSO and P. C. PATNAIK, in Proceedings of American Society of Metals-Materials Week'93, Pittsburg, Pennsylvania, 1993 p. 135.
15. J. L. COCKING, P. G. RICHARDS and G. R. JOHNSTON, *Surf. and Coatings Tech.* **36** (1988) 37.
16. L. SINGHEISER, H. W. GRUNLING, and K. SCHEIDER, *ibid.* **42** (1990) 101.
17. M. G. HOCKING and V. VASANTASREE, *Mater. Sci. Tech.* **2** (1986) 318.

18. S. K. LAU, R. J. BRATTONE and S. Y. LEE, in "High-Temperature Corrosion," edited by R. A. Raps (1981), p. 628.
19. T. AMOS, *Aircraft Eng. Aerospace Tech*. **68**(3) (1996) 23.
20. TERRY FORD, *ibid*. **66**(4) (1994) 5.
21. TERRY FORD, *ibid*. **66**(4) (1994) 5.
22. A. EDWARDS, *ibid*. **67**(1) (1995) 7.
23. C. D. DESFORGES, in "Source Book on Materials for Elevated-Temperature Applications," edited by E. F. Bradley (ASM International, OH, 1979) p. 1.
24. C. P. VIJAYAN, J. HOJO, J. J. HECHLER, B. CHAMPAGNE and S. DALLAIRE, in Proc. Electroless Nickel Conference IV, Chicago, 1985, p. 3.1.
25. Y. LI, *Plating and Surface Finishing* **84** (1997) 71.
26. INDIRA RAJAGOPAL in "Surface Modification Technology," edited by T. S. Sudarshan (Marcel Dekker., Inc. New York, 1989) p.
27. Y. T. PEI, J. H. OUYANGM, T. C. LEI and Y. ZHOU, *Ceram. Int*. **21**(2) (1995) 131.
28. S. WEISSMAN, BENJAMIN POST., M. E. MROSE, H. F. MCMURDIE and M. C. MORRIS, "Search Manual for Selected Powder Diffraction Data for Metals and Alloys, Vol. I-II" (JCPDS, Penn., USA, 1978). The Powder Diffraction File Nos. 17–424, 8–41 & 41A, 27–344, 15–716, 05–682.
29. S. ESKIN, J. ZAHAVI and A. BERNER, *Lasers in Engineering* **84** (1997) 71.
30. HUGH BAKER, "ASM Hand book - Alloy Phase Diagrams, Vol. 3" (ASM International, Materials Park, OH, 1992) p. 2.114.
31. S. M. L. SASTRY, T. C. PENG, P. J. MESCHTER and J. E. O'NEAL, *JOM* **35**(9) (1983) 21.
32. S. H. WHANG, Y. Z. LU and Y. W. KIM, *J. Mater. Sci. Lett.* **4** (1985) 883.
33. Y. M. YIN and C. V. LUPINC, *Scrip. Metall*. **37** (1997) 211.
34. R. RADHAKRISHNAN, S. BHADURI and C. H. JR. HENAGER, *JOM* **49**(1) (1997) 41.
35. K. ITO, M. MORIWAKI, T. NAKAMOTO, H. INUI and M. YAMAGUCHI, *Mater. Sci. Eng A*. **A233** (1997) 33.
36. W. B. JOHNSON and A. S. NAGELBERG, in "Phase Diagrams in Advanced Ceramics," edited by A. M. Alper (Academic Press, Inc. California, 1995) p. 108.

Received 15 April 1999
and accepted 16 February 2000